On-person adaptive evolution of *Staphylococcus aureus* during treatment for atopic dermatitis

Felix M. Key[1,2,+], Veda D. Khadka[1,2], Carolina Romo-González[3], Kimbria J. Blake[4], Liwen Deng[4], Tucker C. Lynn[1,2], Jean C. Lee[5], Isaac M. Chiu[4], Maria Teresa García-Romero[6,#], Tami D. Lieberman[1,2,7,8,#]

Genetic variation among bacterial strains can contribute to heterogeneity in the severity of chronic inflammatory diseases [1,2], but the degree of variation created by *de novo* mutation during colonization is not well understood. The inflamed skin of people with atopic dermatitis (AD) is frequently colonized with *Staphylococcus aureus,* an opportunistic pathogen associated with both asymptomatic colonization of nasal passages and invasive disease[3-6]. While genetic risk and barrier disruption are critical to AD initiation [7,8], *S. aureus* colonization worsens disease severity by promoting skin damage[9]. Here we show, from tracking 25 children treated for AD over 9 months, that *S. aureus* adapts via *de novo* mutations during colonization. Patients' *S. aureus* populations are typically dominated by a single lineage, with infrequent invasion by distant genotypes. Variants emerge within each lineage with mutation rates similar to *S. aureus* in other contexts. Some of these variants replace their ancestors across the body within months, with signatures of adaptive, rather than neutral, forces. Most strikingly, the capsule synthesis gene *capD* obtained four parallel mutations within one patient and was involved in mutational sweeps in multiple patients. We confirm that selection for *capD* negativity is common in AD, but not in other contexts, via reanalysis of public *S. aureus* genomes from 276 people. Our finding of disease-specific selection raises the possibility that adaptation of pathobionts during colonization prolongs the positive feedback cycle of inflammation.

1. Institute for Medical Engineering and Science, Massachusetts Institute of Technology, Cambridge, MA, USA
2. Department of Civil and Environmental Engineering, Massachusetts Institute of Technology, Cambridge, MA, USA
3. Experimental Bacteriology Laboratory, National Institute for Pediatrics, Mexico City, Mexico
4. Department of Immunology, Blavatnik Institute, Harvard Medical School, Boston, MA, USA
5. Division of Infectious Disease, Department of Medicine, Brigham and Women's Hospital and Harvard Medical School, Boston, MA, USA
6. Department of Dermatology, National Institute for Pediatrics, Mexico City, Mexico.
7. Broad Institute, Massachusetts Institute of Technology, Cambridge, MA, USA
8. Ragon Institute, Massachusetts Institute of Technology, Cambridge, MA, USA

+Present address: Max Planck Institute for Infection Biology, 10117 Berlin, Germany (FMK)
#Co-corresponding authors: mgarciar@pediatria.gob.mx, tami@mit.edu

Main

During colonization of human microbiomes, bacteria acquire adaptive mutations that enhance their ability to survive in the human environment, resist antibiotics, and outcompete other strains [10-13]. While these *de novo* mutations rise in frequency due to the survival advantage they provide to the bacteria, their emergence may impact host metabolism, immune homeostasis, or microbiome dynamics. Understanding the tempo and consequences of variations across bacterial genomes is of particular importance for complex inflammatory diseases like atopic dermatitis and inflammatory bowel diseases, for which the causative role of the microbiome has been hard to pin down [14,15]. While recent studies have identified bacterial strains associated with inflammatory states [1,16,17], classic metagenomic approaches do not provide the resolution to robustly identify individual mutations emerging in disease states. As a result, the potential impact of *de novo* microbiome mutations on complex diseases is poorly understood.

Atopic dermatitis (AD) is one such chronic inflammatory skin disease with strong microbial associations and a complex etiology. AD transiently affects up to 20% of people during their lifetime [18] and is particularly prominent among children, who develop itchy patches of inflamed skin, typically located on the cubital and popliteal fossae (inside of elbows and backs of knees) [19]. Genetic and environmental defects in barrier function have been associated with AD, but are insufficient to explain the variation in disease development and response to treatment [20]. Notably, symptomatic AD skin of children and adults is usually colonized by the opportunistic pathogen *Staphylococcus aureus,* with abundance proportional to disease severity [4-6,9,21,22]; this species is usually lowly abundant on healthy skin [23,24]. Its native reservoir is thought to be the nares, where it asymptomatically colonizes 30% of healthy individuals [23]. However, *S. aureus* also causes a variety of human infections of the skin, bloodstream, lung, and bone.

S. aureus sequence types vary in virulence potential, in the antibiotic resistance cassettes they carry, and the disease contexts in which they are most often found (e.g. hospital or community associated) [3,25], yet no sequence types have been robustly associated with AD. A recent study has suggested that *de novo* mutations in a key quorum sensing pathway reduce the risk for healthy babies to develop AD [26]-- supporting a possible role for *S. aureus* mutations beyond the strain level in AD. While *de novo* mutations occurring in *S. aureus* in young children with AD have been observed [27], the fate of these mutations over time and their consequences have not been characterized.

Longitudinal tracking of *S. aureus* evolution in AD

Here, we use longitudinal sampling and culture-based whole-genome sequencing to identify mutations acquired by *S. aureus* that emerge under natural selection on individual people. We conducted a prospective, longitudinal study of 25 children (age 5 to 15 years old) in Mexico with moderate to severe AD at 5 visits over the course of 9 months (**Figure 1a**). Patients were treated for AD during the first 3 months using topical steroids, emollients, and bleach baths and continued treatment at their own discretion before the last follow-up visit (**Supplementary Table 1**). Patients were asked not to take antibiotics during this initial period, but chart review identified that three patients were administered

antibiotics in this initial period due to medical need, and six took antibiotics after this initial period (see **Supplementary Table 1** for details). During each visit, AD severity was assessed using the SCORing Atopic Dermatitis (SCORAD) scale [28], and swabs were collected from seven affected and unaffected skin sites, including cubital and popliteal fossae, forearms and the nares (**Figure 1a**). From each of 225 swabs, we cultured and sequenced up to 10 colonies (Methods), resulting in 1,587 *S. aureus* whole genomes.

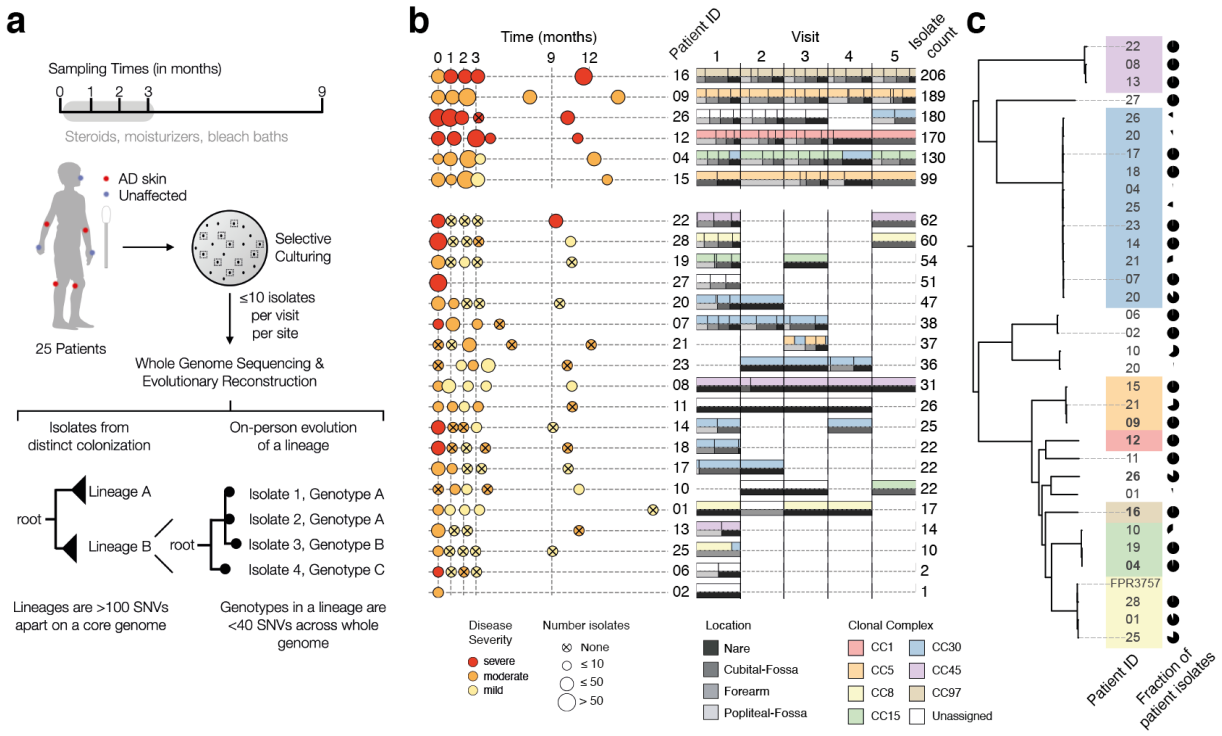

Figure 1: The *S. aureus* population on each child with atopic dermatitis (AD) is dominated by a single, stable, patient-specific lineage. a, Swab samples were collected from each of 7 sites during each of 5 visits, including from nares and areas rarely affected by AD in children (forearms). From each swab, up to 10 colonies were cultured and processed for whole-genome sequencing. We then grouped isolates from each patient into lineages such that isolates from the same lineage are fewer than 100 mutations across the core genome, and performed more detailed evolutionary analysis within each lineage. **b,** Left panel: Sampling time, mean disease severity at visit based on SCORAD (mild < 25 ≤ moderate < 50 ≤ severe), and number of isolates per visit (dot size) are shown for each patient. Right panel: Pairwise stacked bar plots show the inferred clonal complex (top) and sampling location (bottom) for all isolates at each visit. Six patients with ≥ 99 isolates were analyzed with the most detail. **c,** Phylogenetic tree showing the relationship between all 1,551 *S. aureus* isolates sequenced, generated using 60,976 SNVs from a reference-based approach (Methods) and labeled by patient of origin. Pie charts indicate the fraction of patient isolates that come from each lineage, showing most patients have a single major lineage. Patient 20 was colonized by three lineages, two of which are part of the same clonal complex (CC30). Lineages are colored according to their assigned clonal complex (Methods), highlighting that strains colonizing AD patients come from a wide variety of global genotypes.

To understand the minimal number of independent colonizations of *S. aureus* onto each child, we first clustered each patient's isolates into lineages, where each lineage is composed of isolates separated by < 100 mutations across the core genome (**Extended Data Figure 1**). Given the known rates of mutation accumulation in *S. aureus* (~8 mutations/whole genome/yr) [29-34], isolates from distinct lineages are too distant to have arisen from a single colonization and subsequent on-person diversification. Most patients

were stably colonized by a single major lineage, though we recovered minority lineages from 7 patients (**Figure 1b; Supplementary Table 2**).

The *S. aureus* lineages recovered from these patients with atopic dermatitis in Mexico span the diversity of the *S. aureus* species (**Figure 1c**) [35]. The largest fraction of lineages are part of clonal complex 30 (33% of lineages; 15% of isolates), in contrast with a previous finding of clonal complex 1 dominance among people with AD in the UK [27].

The number of isolates analyzed per patient visit is variable and correlates with both disease severity and *S. aureus* relative abundance inferred from 16S rRNA sequencing [22] (0-68 isolates/visit; r^2=0.41 and r^2=0.21, respectively; **Figure 1b** and **Extended Data Figure 2**). While most patients provided isolates from intermittent or single timepoints, six patients suffering from severe AD throughout the study provided large numbers of isolates amenable to quantitative analyses (99-206 isolates/patient; **Figure 1b**).

S. aureus mutants sweep across the body

To analyze the causes and consequences of bacterial mutation on each person, we next focused on the genetic variation within each stably colonizing lineage. For each patient's major lineage, we generated a lineage-specific *S. aureus* assembly, used a rigorous alignment-based approach to identify single-nucleotide variants (SNVs), and built phylogenetic trees that illustrated mutation accumulation on the patient (**Figure 2a-j, Extended Data Figure 3** and **4,** Methods). In many cases, multiple colonies from a timepoint were indistinguishable across their entire genome; we refer to each group of isolates with identical genomes as a 'genotype'.

In theory, the inflammatory environment on AD skin might induce an elevated mutation rate. We estimated the molecular clock of the lineages colonizing the six patients with the most isolates. For five of these patients´ lineages, we observed a fast accumulation of mutations, with molecular clock estimates consistent with those of *S. aureus* in other contexts, including healthy carriage and in invasive infections ($1.2 - 2.7 \times 10^{-6}$ substitutions/site/year [29-34]; **Figure 2b**). Patient 26's major lineage had a substantially higher mutation rate of 3.3×10^{-6} substitutions/site/year (CI95 = $0.1 - 6.4 \times 10^{-6}$ substitutions/site/year), though this difference was not significant. While this non-significantly elevated mutation accumulation rate could plausibly reflect environmental conditions that induced higher mutagenesis, or a defect in DNA repair not apparent in our genomic analyses, we do not observe any significant differences in mutational spectra across patients (**Extended Data Figure 5).** Taken as a whole, these results suggest that AD-associated inflammation does not greatly increase *S. aureus* mutation rates.

Accumulation of mutations in isolates can produce two different patterns of on-person evolution: diversification into co-existing variant genotypes or genotypic replacement. In all six heavily-colonized patients, phylogenetic reconstruction revealed a common pattern in which genotypes with newly acquired mutations repeatedly replaced existing diversity (**Figure 2c-h**). These replacements spanned the entire body; the spread of new mutations was not spatially restricted and included the natural habitat of the nose (**Figure 2i,j, Extended Data Figure 3,4**). While some of these sweeps may have been driven by

antibiotic administration between samplings, many intervals without antibiotic usage demonstrate similarly dramatic changes in mutational composition.

Similar genotypic sweeping likely occurred on most or all patients prior to the start of our study. For all 20 patients with at least 10 isolates at a visit, low diversity co-existed at the earliest such visit, indicating a recent reseeding of the population from a single genotype (< 1.6 years; **Figure 2k**). The frequency at which genotypes replace their ancestors is particularly striking given the stability of on-patient *S. aureus* populations when considered at the lineage level (**Figure 1b**).

Adaptive mutations alter polysaccharide capsule

The speed of genotype replacement raises the possibility that the underlying mutations provide a competitive advantage on AD skin. To test if this process was adaptive, or arose from a neutral bottleneck (e.g. growth following a reduction in cell number during treatment), we investigated mutated genes for adaptive signatures. We first searched for evidence of parallel evolution, i.e. multiple mutations in the same gene within a single patient [36]. In patient 12, we observed four different mutations in *capD,* each in separate isolates. This mutational density is unlikely given the small number of mutations in this patient ($P = 4.3 \times 10^{-5}$, simulation), and all four mutations resulted in either amino acid replacement or a premature stop codon, further supporting an adaptive role for mutations in this gene (**Figure 2i**). The *capD* gene encodes an enzyme that performs the first step in synthesizing the capsular polysaccharide of *S. aureus*. One of the *capD* mutations in patient 12, premature stop codon E199*, is associated with a spread and replacement event in this patient (1 of 11 mutations associated with replacement in this patient). Strikingly, a spread and replacement event in patient 9 is also associated with a mutation in *capD*: a nonsynonymous N595S mutation (**Figure 2j**). While isolates containing this mutation have detectable capsule expression (Methods; **Supplementary Table 3**), this amino acid position is conserved within *S. aureus* and may be critical for native capsule structure (**Extended Data Figure 6**). These observations of parallel evolution within a patient, parallel evolution across patients, and association with replacement events suggest that alterations in *capD* provide a survival advantage for *S. aureus* on AD skin.

We did not detect comparably strong signals of adaptive *de novo* mutation across patients in *S. aureus* genes other than *capD*. Varying selective pressures across patients may have weakened adaptive signatures, and some adaptive events may have been removed by our strict filtering criteria (Putative adaptive signatures, including those associated with sweeps, are listed in **Supplementary Table 4**).

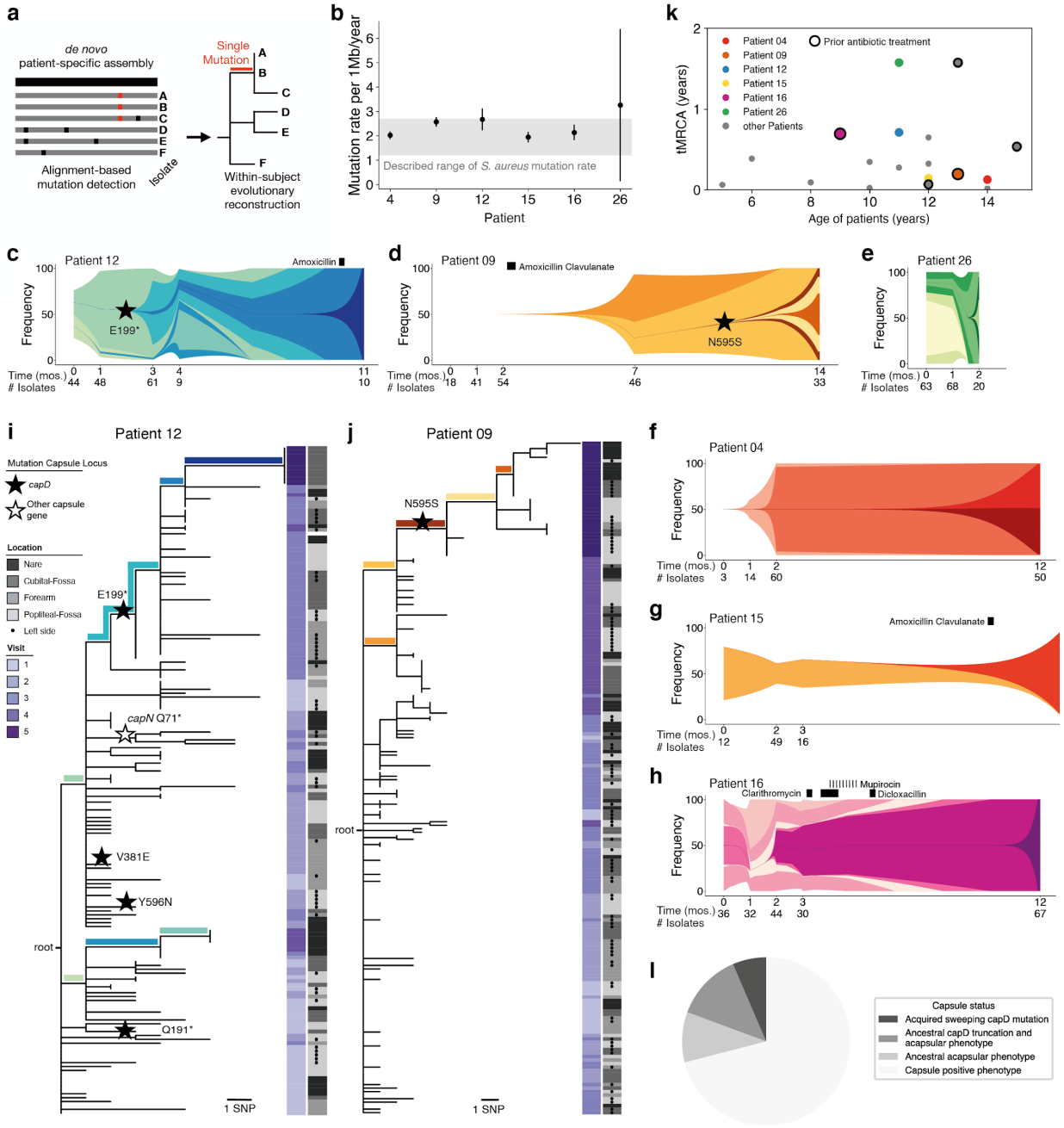

Figure 2. Rapid clonal spread of *de novo* mutations across the body implicates capsule loss as adaptive on treated AD skin. a, We built a *de novo* reference genome for each patient (black) and called *de novo* mutations by aligning raw reads from each sample individually to this reference genome, allowing the building of fine-resolution phylogenetic trees (Methods). **b,** The median molecular clock rate (Linear least-squares regression) is shown for the six patients with the most isolates. Error bars indicate 95% confidence intervals. The gray region indicates rates previously reported for *S. aureus* in other contexts [29-34]. **c, d, e, f, g, h,** Schematics representing the on-person evolution for all patients with $\geq$ 99 or isolates. Each color represents a unique genotype found in at least 3 isolates and with a frequency rise of $\geq$ 30% for at least one visit. The shape and spacing of lines between timepoints with data is modeled based on exponential growth for maximum visibility and speculative (Methods). A star indicates a mutation in *capD.* Black rectangles indicate time and duration of antibiotic treatment. **i, j,** Maximum parsimony tree of evolution of patient 12 (i) and patient 09 (j). The location from which each isolate was taken is indicated in gray (dots indicate left side of body) and timepoint is indicated by the purple heatmap. Stars indicate a mutation

within the capsule locus. Branches representing mutations defining genotypes in panels c and d are colored accordingly. **k,** Recent common ancestors are common across all patients in our study independent of antibiotic use. For each patient, the inferred time elapsed since the population's most recent common ancestor (tMRCA; Methods), using the earliest timepoint for which at least 10 isolates were available, is plotted relative to the patient's age. Any patient that received antibiotic treatment before that visit is shown with a black outline. Mutational distances were converted to time using the calculated molecular clocks for the 6 highlighted patients; for all others, the median rate was used. **l,** Pie chart indicating the capsule status for 33 major and minor lineages recovered from 25 patients. Sweeping capsule mutations were observed in 2 patients' *S. aureus* populations, 4 lineages were determined genetically and by *in vitro* phenotyping to have lost the capsule prior to the start of our study, and 3 lineages were determined capsule-negative by *in vitro* phenotyping only (**Supplementary Table 3**).

Notably, we did find a signature of adaptive maintenance of mobile elements (**Extended Data Figure 7**). While isolates from the first visit of several patients consisted of a mix of those with and without mobile elements (including prophages and plasmids; **Supplementary Table 5**), all mobile elements detected at a patient's first visit were found in all isolates at their last visit sampled.

Capsule loss is common in AD globally

The polysaccharide capsule of *S. aureus* has been well studied, and it is generally considered a virulence factor that shields the pathogen from phagocytosis and the innate immune system [37-39]. However, the loss of the *S. aureus* capsule has been observed previously to emerge *in vitro* and *in vivo*[40,41], including the epidemic USA300 clone, and it has been shown that capsule-negative *S. aureus* exhibits improved adherence to fibrinogen, platelets, and endothelial cells [42-44]. The adaptive emergence of *capD* truncation mutations on AD skin suggests an advantage for the acapsular phenotype on AD skin.

We next sought to understand the generality of selection for *capD* alterations in our cohort. It is possible that replacement events involving *capD* emerged prior to the start of our study, given our inference of recent replacement events (**Figure 2k**). Alternatively, a patient's *S. aureus* population may have been initially founded by a strain with a nonfunctional *capD*. We tested all patient isolates for a complete *capD* open-reading frame and observed that the major lineage of four additional patients had ancestral truncation mutations in this gene. Three of these patients share the same frameshift mutation (single base insertion at an adenine hexamere of *capD*) also found in many CC8 strains, indicating that this mutation was carried on their founding strains. The remaining lineage had a unique *capD* truncations (10 bp deletion). We also searched for capsule loss driven by non-truncation mutations or mutations in other genes by performing immunoblots, which identified two additional major lineages without detectable polysaccharide capsule *in vitro.* In total, 24% of the major lineages were acapsular at enrollment (**Figure 2l, Supplementary Table 3**).

To better understand whether loss of *capD* is generally beneficial for *S. aureus in vivo* or specifically advantageous on AD skin, we leveraged publicly available genomes of isolates from people with and without AD. We analyzed 276 *S. aureus* isolate whole-genomes from 110 AD patients, 67 healthy carriers, and 99 individuals who had other infections (blood-stream, soft tissue, bones, and joint; **Figure 3a**) [27,45-47].These samples were collected from individuals in Denmark, Ireland, and the UK.

Strikingly similar to our observation that 24% of AD patients carry a strain encoding a truncated CapD, 22.5% of AD-associated isolates in the public data lack a full-length *capD* gene. This represents a significant increase relative to isolates from healthy controls (7.2%, $P < 0.001$; one-sided Fisher's exact

test) and from those with other types of infections (10.5%, P = 0.020) (**Figure 3b**). Phylogenetic analysis confirms several independent emergences of *capD* truncations, supporting the notion that *de novo* loss of *capD* can drive *S. aureus* adaptation (**Figure 3c**). Notably, 78% of capD-truncation isolates come from two independent, globally successful clones with recent expansions, including a CC8 clade from which USA300 is descended and a CC1 clade with a large deletion spanning *capD-capH.* Nevertheless, the observed signal remains significant when isolates from CC8 are excluded (AD vs. healthy: P < 0.001, AD vs. other infection: P = 0.016) and when the entire dataset by Edslev et al. [46] is removed, which included most of the CC1-*capD* negative isolates (AD vs. healthy P = 0.014). Furthermore, when considering all genes in the capsule locus, we observe an even stronger statistical enrichment of truncation mutations in isolates from AD (P < 0.001, vs. healthy; **Extended Data Figure 9c**). These robust genomic differences indicate that selective pressures felt by *S. aureus* on AD skin are distinct from those on healthy patients or in the context of acute infection.

To understand if capsule loss via mutations in other genes is also enriched in AD, we repeated the same analysis for genes known to be associated with capsule regulation [48,49]. Interestingly, *agrC*, the histidine-kinase sensor in the *agr* quorum-sensing-dependent virulence regulation system, also showed a significant enrichment of independent loss-of-function mutations in AD compared to other infections (P < 0.001) but not isolates from healthy patients (**Figure 3d**; **Extended Data Figure 8**). While recent work has suggested that retention of functional *agr* is associated with the onset of AD [26], *agrA* loss has been previously documented on the skin of a patient with AD [27]. Loss of the *agr* system is known to suppress capsule production, among other virulence-associated pathways [48,50]. While the selective advantage driving frequent *agr* loss in AD could be independent of capsule, this observation is consistent with an advantage for an acapsular phenotype on AD skin.

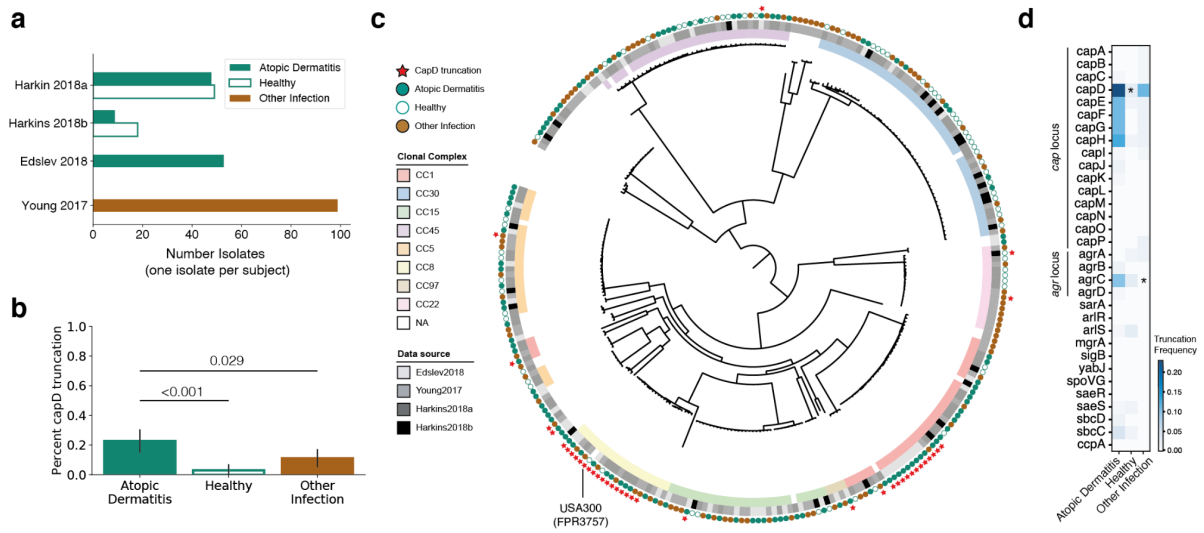

Figure 3. Meta-analysis of published data confirms enrichment of capsule loss on AD skin. a, The number of *S. aureus* genomes downloaded from each of 4 public studies are shown [27,45-47]. Isolates were collected either from people with AD (green), healthy individuals (white), or from a variety of other diseases, including bloodstream, bone/joint and soft-tissue infections (brown). **b,** The fraction of isolates with a truncated or missing *capD* is plotted as a function of isolation context. The 95% binomial proportion confidence interval is shown. **c,** Phylogenetic tree showing relationship between all *S. aureus* analyzed, generated using a reference-based approach and maximum-likelihood reconstruction (Methods). Isolates are labeled

with squares indicating their membership in global lineages and the study of origin, with circles indicating isolation context. Red stars indicate isolates without a full length *capD,* showing 9 different independent occurrences including two expanded clades. **d,** Analysis similar to that in (b) was performed for other genes involved in capsule regulation, and the percentage of isolates from each context lacking a full length copy of each gene is shown as a heatmap. * $P < 0.001$ vs. AD (one-sided Fisher's exact test).

What is the mechanistic basis of acapsular advantage on AD skin? Possible, non-mutually exclusive, selective pressures for capsule loss include: (1) immune escape from capsule-targeted antibodies or innate immune components; (2) increased adherence to AD skin via improved accessibility of surface adhesin proteins; and (3) alleviation of metabolic costs. Antibiotic resistance is unlikely to be a driver of capsule loss, as resistance-associated genomic features were generally depleted from isolates from AD context in our meta-analysis, with the exception of fusidic acid (**Extended Data Figure 9**) -- a common topical antibiotic whose efficacy we confirmed is not impacted by capsule negativity (MIC 0.05ug/mL for all strain pairs tested from P9 and P12; Methods). Further, no emerging resistance is associated with the acapsular phenotype observed in our patient data, despite occasional antibiotic treatment (**Extended Data Figure 10**).

Metabolic cost may explain the preponderance of mutations in *capD* -- the first gene in the biosynthetic pathway -- rather than an even distribution across all capsule-associated genes. To understand the cost of capsule production, we measured growth rates in rich media, and found that acapsular isolates grew 1.4 - 2% faster than their capsular ancestors (an advantage amplified over multiple generations; Methods; **Extended Data Figure 11**). However, this growth advantage did not translate to significantly worse disease or bacterial loads in acute mouse models of skin damage and colonization (< 1 week; **Supplementary Note**; Methods). Additionally, three AD isolates with point mutants that did not abrogate the capsule entirely did not show a growth advantage (**Extended Data Figure 11**). Together, these data suggest additional selective pressures on AD skin that were not apparent in our mouse models, possibly due to the short duration of the *in vivo* experiment. The ability of acapsular strains to evade antibodies [51,52] and increase adhesion [42-44] have been demonstrated in mouse models of other infections and may play a role during long term colonization on humans.

Discussion

S. aureus is among the most successful opportunistic pathogens of humans, colonizing a third of the world's population, responsible for numerous outbreaks in healthcare facilities, and causing a variety of acute and chronic diseases[3]. Here, we report that *S. aureus* rapidly adapts via *de novo* mutations on people being treated for AD, and that loss-of-function mutations in a *S. aureus* gene closely associated with virulence, *capD*, are frequent on AD, but not healthy, skin.

Loss of function mutations in *capD* are present in global lineages, yet new bacterial genotypes with mutations in this gene also arise on individual patients with AD, spread across a patient's skin, and replace their ancestors within months. Our finding that loss of function in the capsule pathway is associated with AD is surprising in the lack of a consistent signal in AD-association at the level of sequence types, clonal complexes, or other phylogenetic groupings. The discrepancy across scales of

genomic units suggests that ecological dynamics (e.g. priority effects[53]) or selective tradeoffs limit the specialization ability of *S. aureus*.

At a global scale, the advantage of being acapsular on skin may in part explain the success of the acapsular *S. aureus* USA300 lineage in causing skin infections and spreading to epidemic levels outside the hospital[40]; future studies are needed to test whether acapsular mutants have an increased capacity for inter-person spread.

We cautiously propose that small molecules or other therapies that specifically target *S. aureus* strains without a functional capsule locus might be combined with selective forces on the host to lower the burden of *S. aureus* colonization in AD. Future work further characterizing the mechanistic basis behind the CapD-negative advantage on skin will be critical to the design of such therapies, as unexpected consequences may emerge from selection for the capsular phenotype, which is more virulent in other disease contexts[37,54].

This study focused on *S. aureus* genotypes that could be easily recovered from swabs at 7 body sites. We did not seek to characterize community members at low abundance, and it is possible that additional minority lineages and genotypes were present at undetected levels or at additional locations on the body (**Extended Data Figure 12**). We note that similar limitations exist for culture-independent approaches, as it is difficult to distinguish between sample cross-contamination and low abundance colonization [55]. Our data support a model in which lineages can persistently colonize despite lack of detection; we recover the exact same lineages from four patients (**Figure 1b**) after visits at which no *S. aureus* was recovered. Phylogenetic reconstruction is consistent with persistence on the patient (**Extended Data Figure 4**), though intrafamily transmission cannot be ruled out. All patients were treated for AD via emollients and steroids, and some patients received antibiotics or took bleach baths during the study period (**Supplementary Table 1**). Therefore, these observations of mutational speed and adaptive events may not be applicable to untreated AD skin.

Together, our results highlight the potential of *de novo* mutations for altering bacterial competitiveness in microbiomes, highlight the power of mutation tracking for identifying new therapeutic directions, and suggest that whole-genome resolution may be required for predicting the impact of microbial strains on complex diseases.

Methods

Study cohort and sample collection

Patients were recruited from the Dermatology Clinic at the National Institute for Pediatrics in Mexico City under a protocol approved by the Institutional Review Boards of the NIP (042/2016) and Massachusetts Institute of Technology. Inclusion criteria for enrollment were: ages 5 to 18 years, diagnosis of AD according to modified Hanifin and Rajka criteria [56] and SCORAD ≥ 25 at first visit. We preferentially enrolled patients that had not taken topical or systemic antibiotics for the past month, though one patient (Pt 15) did take antibiotics immediately prior to enrollment. Overview of patient data, including treatment, is in **Supplementary Table 1**. Skin swabs were collected from seven different locations at up to 5 visits (**Figure 1A**), placed in Liquid Amies transport media, and sent to the laboratory for culture. Swabs were directly inoculated on mannitol salt and blood agar plates and cultured for 24h at 37℃. For each culture plate, up to 10 colonies suspected to be *S. aureus* by colony morphology were selected. These colonies were restreaked on ¼ of a blood agar plate and cultured for 24h at 37℃ to obtain sufficient material for DNA extraction. DNA was extracted using the Wizard® Genomic DNA Purification Kit (Promega Corporation) for Gram-positive bacteria.

Dual-barcoded DNA libraries were constructed using the plexWell library prep system (SeqWell) for most samples and a modified version of the Nextera protocol for a small subset[57]. Libraries were sequenced on the Illumina NextSeq 500 using paired end 75bp reads to average of 3.1M reads per isolate (75 bp paired end). Demultiplexed reads were trimmed and filtered using cutadapt v1.18 [58] and sickle-trim v1.13 [59] (pe -q 20 -l 50).

We note that sequenced *S. aureus* genomes from each patient is an imperfect measure of *S. aureus* absolute abundance. In some cases with heavy growth, it was difficult to isolate 10 colonies. In addition, not all cultured isolates yielded sequenceable libraries due to a failure in DNA extraction or library prep, and some sequenced colonies were determined not to be *S. aureus* from genomic data and excluded from the analysis. Regardless, we find good correlation between colony count data and relative abundance inferred from 16S rRNA sequencing (**Extended Data Figure 2**).

Assignment of isolates to lineages

Reads were aligned using bowtie2 v2.2.6 (-X 2000 --no-mixed --dovetail) against methicillin-resistant *Staphylococcus aureus* USA300-FPR3757 (RefSeq NC_007793). Candidate single nucleotide variants were called using samtools (v1.5) mpileup (-q30 -x -s -O -d3000), bcftools call (-c), and bcftools view (-v snps -q .75) [60,61]. For each candidate variant, information for all reads aligning to that position (e.g. base call, quality, coverage), across all samples, were aggregated into a data structure for local filtering and analysis. Isolates were removed from analysis if they had a mean coverage 7 or below across variant positions (208 isolates of an initial 1,787). Sporadic isolates that were phylogenetically confined within the diversity of another patient were likely mislabeled and removed (7 isolates). Isolates with a mean minor allele frequency above 0.03 across candidate sites (indicates contamination) were removed (21 isolates). We filtered candidate SNVs using a publicly available protocol (see Data Availability) similar to that previously published [36]. Basecalls were marked as ambiguous if the FQ score produced by samtools was below 30, the coverage per strand was below 2, or the major allele frequency was below 0.85. Remaining variant positions were filtered if 5% or more of all isolates were called as ambiguous (this

removes most of the 'accessory' genome) or if the median coverage across strains was below 3, or if no unmasked polymorphisms remained. Any isolates for which ≥10% of candidate positions were marked as ambiguous at this stage were removed, presumably due to impurity of the starting colony (this removed no additional isolates, leaving 1,551 isolates). These filters retained 60,976 SNVs across 1,551 isolates. A maximum-likelihood tree was built with RAxML v8.2.12 [62] using the GTRCAT model, with rate heterogeneity disabled (-V). The phylogenetic tree was visualized with iTol [63]. For each isolate the sequence type and clonal complex was inferred using SRST2 [64] and the *S. aureus* MLST/CC database was obtained March 2020 (with 5,964 sequence types) [65]. All 25 isolates from patient 17 were manually assigned to CC30 after failing SRST2 clonal complex assignment, despite allele types matched for 6 out of 7 alleles to CC30. The CC30 is also confirmed by the phylogenetic placement for patient 17. All other isolates that failed sequence typing were ignored for CC-dependent analysis (67 out of 1,551). Lineages are defined as phylogenetically closely related *S. aureus* from the same patient which differ by less than 100 SNVs on the core genome. Analysis of minor lineage detection dependency on the number of isolates sampled at a given visit suggests that deeper sampling would have been unlikely to detect additional lineages from patients (**Extended Data Figure 2c**). A second phylogenetic performed using the methicillin-sensitive *S. aureus* FDA209P (NCTC 7447, RefSeq NZ_AP014942, NZ_AP014943) genome as a reference for alignment [66] resulted in the same lineage groupings (data not shown).

Within-patient phylogenetic reconstruction using *de novo* assemblies

We constructed patient-specific assemblies in order to capture true genome-wide diversity; this approach can capture genetic information only found in a single isolate [13]. Filtered reads were taxonomically assigned using kraken2 (standard database build Sep 24 2018) [67], and only isolates with ≥ 80% reads assigned to *S. aureus* on the species level were included for *de-novo* assembly, leaving 1,271 isolates. For each lineage, we concatenated up to 250,000 reads from each member isolate and assembled a reference genome with SPAdes [68] (v3.13, careful mode). For patients colonized by multiple lineages we only analyzed isolates from the major lineage. All scaffolds of size 500b or larger were annotated using prokka [69] (v1.14.6), which was supplied with a list of proteins (*--proteins*) from nine publicly available *S. aureus* genomes and six accompanying plasmids (NCBI accession: NC_002745, NC_003140, NC_002758, NC_002774, NC_009641, NC_003923, NC_002952, NC_002953, NC_005951, NC_002951, NC_006629, NC_007795, NC_007793, NC_007790, NC_007791, NC_007792). The assemblies for each patient are summarized in **Supplementary Table 6**.

We aligned the data of all initial 1,768 isolates to their respective patient-specific assemblies using bowtie2 [70] using the same parameters as described for *assignment of isolates to lineages* analysis. Isolates were removed if phylogenetically identified as minor lineages (62) or cross contaminants (30). Isolates and candidate single nucleotide variants were processed similar to the *assignment of isolates to lineages* calling, but without an isolate filter based on minor allele-frequency and base call-frequency. To remove isolates with an inflated mean coverage across the assembled genomes due to high-copy number plasmids we required in addition at least 10% of the genome covered at 8X. To detect variations within the accessory genome, the allowed maximum fraction of ambiguous isolates per site was increased from 5% to 25%. To remove variants that emerged from recombination or other complex events, we identified SNVs that were less then 500b apart and covaried highly across isolates within a patient (a SNV was considered to highly covary with another SNV if its covariance was in the 90% percentile across covariances calculated with the focal SNV); these positions were removed from downstream analysis.

Patients left with less than two isolates or SNVs were not analyzed. Across all patients we analyzed in total 1,456 isolates with 955 *de novo* on-person SNVs (**Supplementary Table 7**). Phylogenetic reconstruction was done using *dnapars* from PHYLIP v3.69 [71]. Trees were rooted using the isolate with the highest coverage from the most closely related lineage (based on *assignment of isolates to lineages* analysis) as an outgroup.

Signatures of within-person adaptive evolution

Each within-patient dataset was searched for genes with either of two signatures of adaptive evolution: parallel evolution at the gene level [10] and hard selective sweeps [72-74]. First, we identified cases when two or more mutations arose in a single gene within a patient, with a minimum mutation density of 1 mutation per 1000 bp. We calculated a p-value for enrichment of mutations in each gene using a Poisson distribution. Only the *capD* gene in patient 12 had a significant p-value after Bonferroni correction for the number of genes on the genome (**Supplementary Table 4**). Second, we searched for genomic positions at which the mutant allele frequency rose by at least 30% between visits. For each SNV, we assigned the ancestral allele as the allele found in the patient-specific outgroup, or, if that was not available, we used the allele present in the patient-specific assembly. We compared lists of genes with candidate adaptive signatures across patients using CD-HIT (v4.7, 95% identity)[75]. All candidate signatures of adaptive evolution are reported in **Supplementary Table 4**.

Creation of evolution cartoons (Muller plots)

We visualized the change in frequency of mutations observed on each patient with ≥99 isolates using Mueller plots. Patient 04 and patient 15 yielded only two isolates at visit 3 and visit 2, respectively; these were omitted from visualization. We only drew mutations with an observed variation in frequency of ≥0.3 between timepoints. We converted mutation frequencies into genotype trajectories using *lolipop* v0.8.0 (https://github.com/cdeitrick/Lolipop), SNVs that differed by less than 8% derived allele frequency across timepoints were grouped into a single genotype. To make successive sweeps more visible, we used a custom-made python function to generate intermediate genotype frequencies between sampling timepoints. In brief, we created 100 time units per month, assumed mutations swept sequentially, and applied an exponential growth or decline following the function of frequency $x = \mathcal{E}\text{^}((\ln(f_1) - \ln(f_0)) / g)$, with f_0 is the frequency at preceding visit or 0, f_1 is the frequency at the next visit and g is the number of time units (see code availability). The extended table was used again as the input for *lolipop*, which provided the input tables for plotting using the R package *ggmueller* v0.5.5 [76].

Molecular clock and TMRCA

We estimated the number of *de novo* mutations per isolate using all positions variable within a patient lineage. The ancestral state of each variant is defined by the allele called in the lineage-specific outgroup. If this was not available, the major allele for all non-patient outgroup isolates was used. Only for patient 26 we adjusted the outgroup manually in order to fit the molecular clock best according to *treetime* [77], by changing the ancestral allele at four basal mutation positions. We normalized the number of mutations per isolate by dividing by the number of positions on the reference with a depth of at least 8X. We inferred the molecular rate using linear regression implemented in scipy v.1.3.1 [78]. Time to the most recent common ancestor (tMRCA) was calculated for each patient data from each patient's earliest visit with at least 10 isolates. For each of the five highly colonized patients the tMRCA was calculated using their inferred mutation rate, while for all other patients the median molecular rate of the six highly colonized individuals was used (2.36×10^{-6} substitutions/site/year).

Mobile genetic element analysis

We identified genetic gain and/or loss events based on the depth of coverage of each isolate aligned to its patient-specific assemblies along the six individuals with at least 99 isolates. To avoid spurious results due to uneven coverage across samples or genomic regions, we calculated a z-score for each position by normalizing each isolate's depth of coverage at each position by sample and by position. We identified genomic regions greater than or equal to 5,000 bp long, for which each position's z-score was below a threshold of -0.5 with a median threshold below -1.0. Identified candidate regions were further filtered to have at least one isolate with a median coverage of 0 and at least one with an average depth of at least 10X. Candidate regions were confirmed using a custom, semi-automated python module that allowed interactive validation of each candidate (**Supplementary Table 5**).

Capsule typing

S. aureus capsule serotyping was performed as described previously [79]. Briefly, duplicate tryptic soy agar plates were spot inoculated in a grid pattern with *S. aureus* isolates and incubated overnight at 37°C. The colonies were blotted onto nitrocellulose filter membranes for 5 min at ambient temperature. Adherent colonies were fixed to the membranes by heating them at 60°C for 15 min. After two washes with 10 mM sodium phosphate buffer-0.85% sodium chloride (phosphate-buffered saline; PBS) to remove excess cells, the filters were immersed in a solution of trypsin (1 mg/ml; Sigma) for 60 min at 37°C to remove protein A from the bacterial cells. After two washes in PBS, the filters were blocked with 0.05% skim milk for 1 h and washed in PBS containing 0.05% Tween 20 (PBST). Each filter was incubated with capsule type-specific rabbit polyclonal antisera (diluted 1:4,000 in PBST) at 37°C for 1 h. After washing in PBST, horseradish peroxidase-conjugated donkey anti-rabbit immunoglobulin (diluted 1:5000) was incubated with each filter for 1 h at 37°C. After three washes, KPL 1-Component TMB Membrane Peroxidase Substrate was added to the filters. A purple color developed within 5 min and was scored visually from 0 to 4+. The reactivities of the clinical isolates were evaluated by comparison with those of control *S. aureus* strains (serotypes 5, 8, and nontypeable isolates) included on each filter. Results are presented in **Supplementary Table 3**.

Growth rate

Overnight cultures were inoculated into fresh TSB at a 1:100 dilution. Cultures were grown at 37℃ with shaking, for 24h in a Tecan plate reader (Infinite F Nano+, Tecan Trading AG, Switzerland). Absorbance at 595 nm was measured every 5 minutes. The plate containing growing cultures was sealed using its own lid. The growth rate was calculated using a regression on log-normalized data.

All experiments were performed with representative bacterial - test - isolates carrying *de novo* mutations in the *capD* gene from patients enrolled in this study. For each test isolate, a phylogenetically closely related and basal control isolate was chosen. Sometimes the test isolate contained 1-2 additional mutations compared to the most closely related basal isolate observed.

Fusidic Acid Susceptibility

Overnight cultures of patient isolates of *S. aureus* were diluted and plated on varying concentrations of fusidic acid (Sigma-Aldrich), ranging from 0.02ug/Ll to 2.5ug/mL. Both capsule positive and capsule negative strains were found to be susceptible at 0.05ug/mL, although the emergence of resistant mutants was common.

Public *S. aureus* isolate sequencing data analysis

We investigated publicly available data to verify if loss of CapD is associated with *S. aureus* colonizing AD skin. We obtained whole-genome sequence data from 4 different publications analysing *S. aureus* in healthy individuals, AD patients or individuals with other *S. aureus* infections [27,45-47]. When data from multiple isolates per patient was available, we used only one isolate in order to assess prevalence of variants across conditions; the isolate with highest coverage was chosen. To understand the relationship between isolates, we performed an alignment-based phylogenetic reconstruction using *S.aureus* COL (sequence version number: NC_002951.2, NC_006629.2) using the same filters as above. To examine gene content, we performed *de novo* assembly for each isolate using SPAdes (v3.13, --careful) [68] and annotated the assembly using Prokka (v1.14.6) [69] as described above. We removed 6 isolates with an assembly length of < 2.6M nucleotides. In total, we analysed 276 isolates from 276 patients. In addition, we included USA300-FPR3757 (RefSeq NC_007793) as a sample, by simulating raw reads for input to our cross-lineage phylogenetic analysis (cutting its genome in segments of size 150 b in steps of 1 b to simulate reads). The maximum likelihood phylogeny was built using RAxML v8.2.12 (-m GTRCAT) [62] and visualized with iTol [63].

We inferred the ORF status for all capsule and capsule-associated genes using the annotated assemblies and BLAST+ v2.7.1 [80]. Details about each query gene are available in **Supplementary Table 8**. We compared the best BLAST match for an overlap with the annotated reading frame. We accepted an ORF as complete if the start and end of the best BLAST hit were each within 100 bp of a gene start or end of a gene in the annotated assembly. *S. aureus* genomes colonizing humans are known to carry 1 of 2 predominant *cap* loci (type 5 or 8) [37] and 1 of 4 *agr* types [81] containing homologous versions of the same genes; for these cassettes we performed analysis only for the respective loci with the best BLAST match to a given isolate. Results are reported in **Figure 3**, **Extended Data Figure 8** and summarized in **Supplementary Table 9**. When only data from publications reporting both AD and controls are included, the enrichment of *capD* premature stop codons in AD vs controls remains significant (P=0.026).

Collectors Curve Analysis

For each patient's sampling point (visit) with at least 10 isolates a collector curve was created for dMRCA or identified SNVs (Extended Data Figure 12). For each patient-visit dataset we re-sampled with replacement $0 < x < n$ isolates each x sampled 100 times, calculated the within-sample diversity, and plotted the mean and standard deviation.

Author contributions

M.T.G-R. and T.D.L designed the clinical cohort. M.T.G-R. enrolled patients and collected clinical samples. C.R-G. cultured bacteria from clinical samples and extracted DNA. T.C.L. and T.D.L. prepared genomic libraries. F.M.K. and T.D.L performed genomic analysis and interpretation. J.C.L. performed

capsule assays and provided *S. aureus* strains. V.K., K.J.B, L.D., and I.M.C. performed mouse experiments. V.K. and L.D. performed *in vitro* experiments. F.M.K. and T.D.L wrote the manuscript with feedback from all authors.

Acknowledgements

We thank Mariana Matus and Eric Alm for assistance in the design of the clinical cohort, the BioMicroCenter at MIT for performing genomic sequencing, Samantha Choi for technical support on animal experiments, Paul F. Koffi for performing *in vitro* capsule immunoblots, Chris Manusco and Calen Mendall for experimental assistance and members of the Lieberman lab for valuable advice and feedback on the manuscript. We acknowledge support from MISTI Global Seed Funds (to T.D.L. and M.T.G-R.), the National Institutes of Health (DP2-GM140922 to T.D.L., R01AI30019 to I.M.C.), Burroughs Wellcome Fund (to I.M.C.), the Mexican Government Ministry of Taxes Program E022 for Health Research and Technological Development 2018 (to M.T.G-R.), and DFG research fellowship (KE 2408/1-1 to F.M.K.).

Competing interests

No competing interests to declare.

Data availability

All raw data is available at SRA under BioProject identifier: PRJNA715375, PRJNA715649, and PRJNA816913. Metadata of each isolate including SRR identifier is available in **Supplementary Table 10**.

Code availability

All code needed to reproduce the results of this study, including snakemake pipelines, are available here: https://github.com/keyfm/aureus_ad.

Extended Data Figures

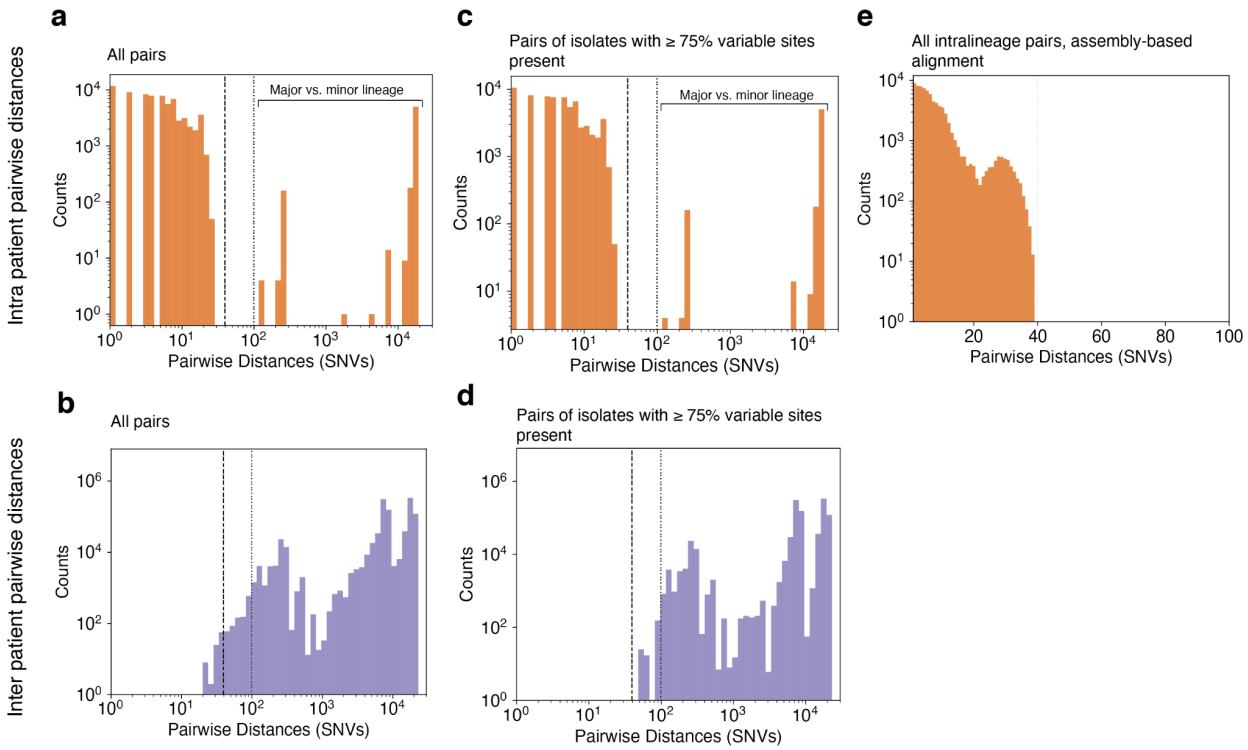

Extended Data Figure 1. Whole-genome pairwise distances between isolates of the same patient, or between patients, enables differentiation of lineages. a. Histogram of pairwise distances between isolates within a patient. Isolates from the same lineage have fewer than 30 SNV differences across the core genome using an alignment-based approach (reference genome: USA300-FPR3757). Both axes are on log scale to make major-minor lineage pairs more visible. **b.** Histogram of pairwise distances between isolates of different patients. We note that some pairs of isolates from different people were also separated by less < 100 SNVs (e.g. on CC30) across their core genomes using an alignment-based approach (reference genome: USA300-FPR3757); however these pairs included isolates with relatively low coverage. **c,d.** When isolates are only included in this analysis if they have at least 75% (45,742 SNVs) of all identified variable sites with coverage of 8X using an alignment-based approach (reference genome: USA300-FPR3757), a more clear separation between intra-patient and inter-patient diversity is seen at 40 SNVs (vertical dotted bar). The existence of inter-patient pairs with small distances relative to the molecular clock of *S. aureus* suggests spreading of *S. aureus* in the community within the past few years; we note that all of these pairs are within CC30. Both axes are on a log scale to enhance visibility. **e.** Histogram of pairwise differences observed among isolates of major lineages aligned to their respective assembly-based reference genome. The Y axis is on a log scale to enhance visibility. Black, vertical dashed line indicates 40 pairwise differences; black, vertical dotted line indicates 100 pairwise differences.

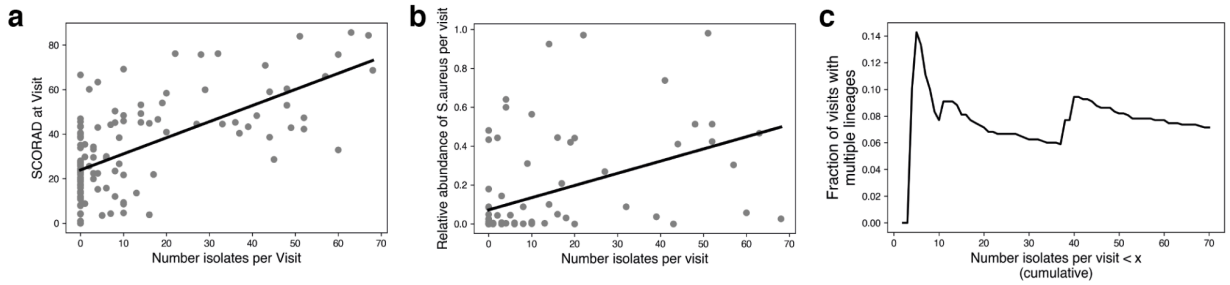

Extended Data Figure 2. Number of recovered isolates correlates with disease severity and relative *S. aureus* abundance per visit but not with the detection of multiple lineages. **a.** Linear least-squares regression for the number of recovered isolates and disease severity (SCORAD) per visit (r^2=0.41) demonstrates a relationship between disease severity and the number of isolates recovered. **b.** Linear least-square regression for the relative *S. aureus* frequency (16s rRNA; averaged across sites) and number of recovered *S. aureus* isolates per visit demonstrates a relationship between the relative abundance of *S. aureus* and the number of isolates recovered (r^2=0.21). The 16S rRNA data was originally described in Khadka et al. [22]. **c.** Fraction of visits where more than 1 lineage was detected on a patient demonstrates a lack of relationship between detection of minor lineage and number of isolates cultured. Also see **Extended Data Figure 12**.

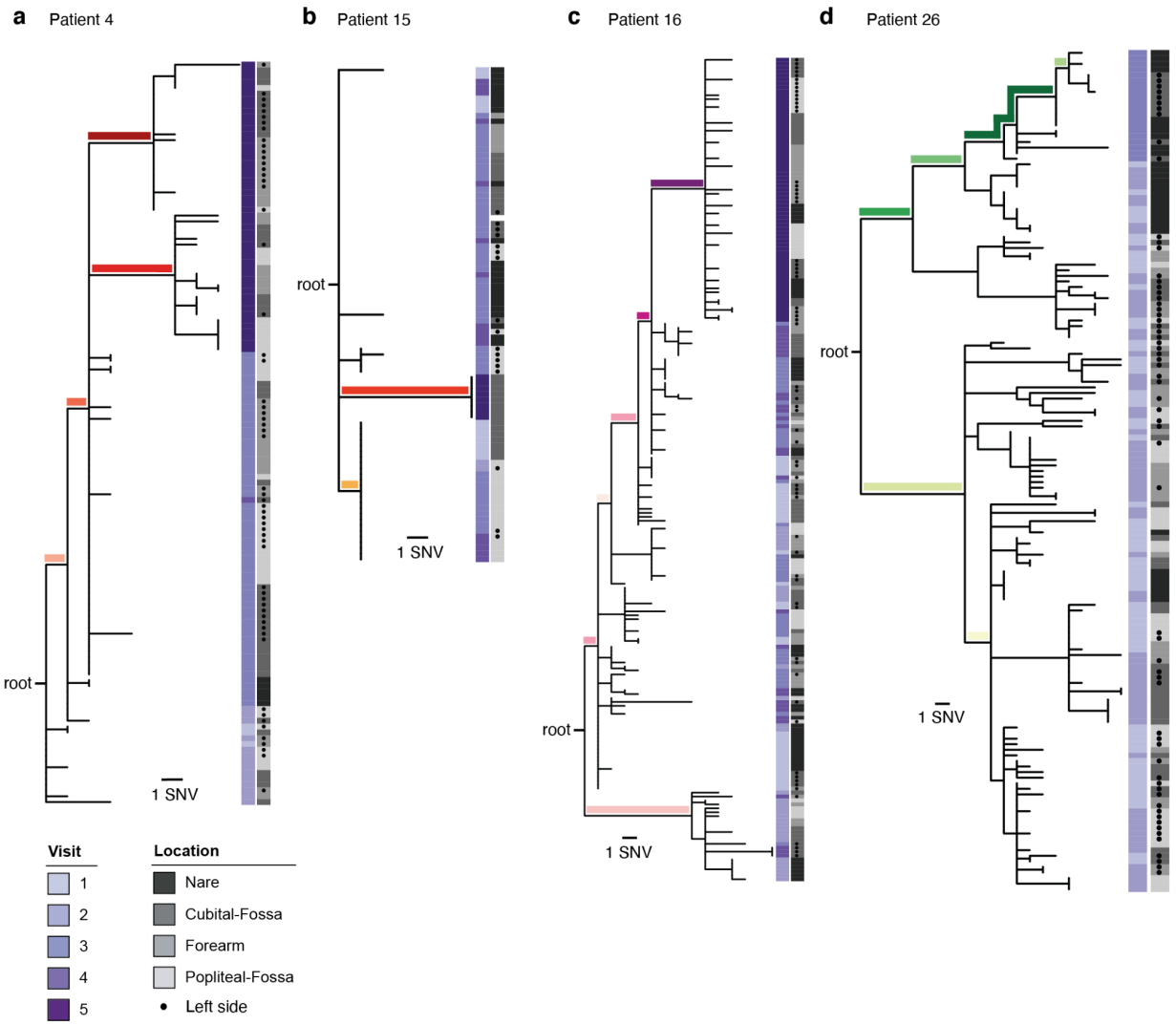

Extended Data Figure 3. Within-patient evolutionary reconstruction of *S. aureus* for other highly colonized patients. Within-person evolutionary trees for Patients 04 (**a**), 15 (**b**), 16 (**c**) and 26 (**d**), constructed similarly to **Figure 2i/j.** The location from which each isolate was taken is indicated in gray (dots indicate left side of body) and timepoint is indicated with the purple heatmaps. Branches with >30% change in frequency between timepoints are colored in accordance with **Fig**ure **2c-h**.

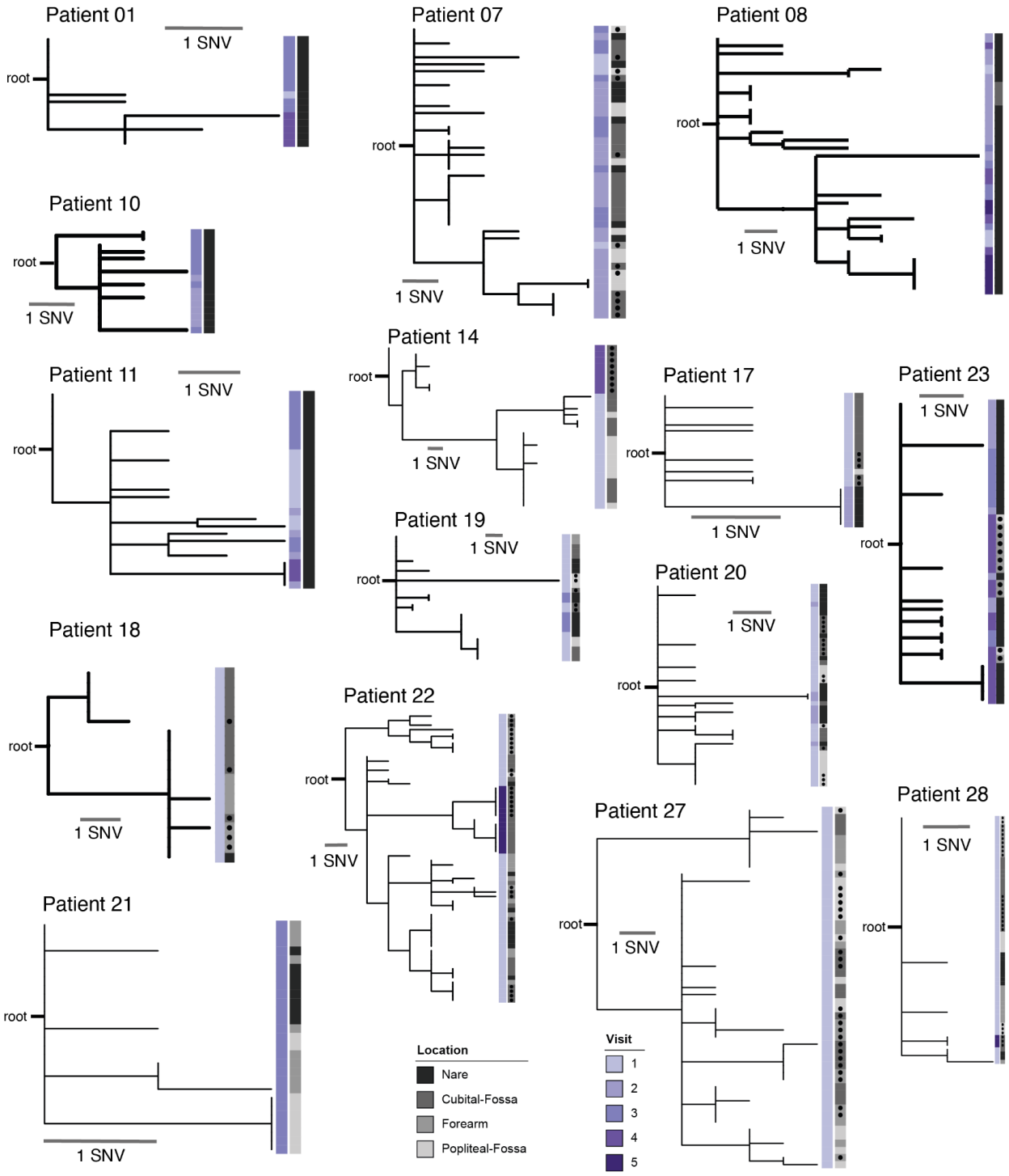

Extended Data Figure 4. Within-patient evolutionary reconstruction of *S. aureus* genomes recovered from patients with less than 99 isolates. The patient-id, root, and branch length is indicated for each phylogeny. Sampling visit is shown in shades of purple and sampling location of where an isolate was collected is shown in shades of gray (dot indicates left side of body).

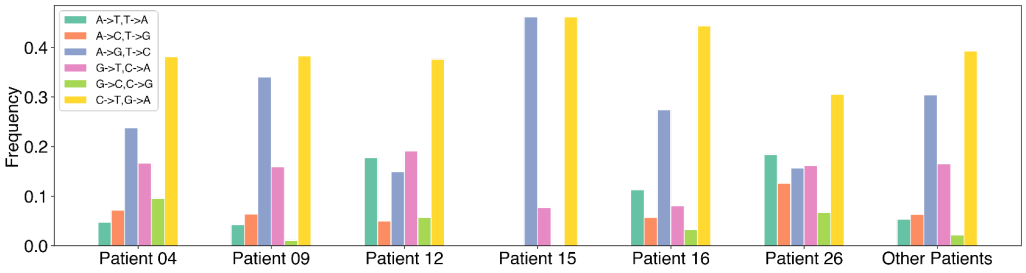

Extended Data Figure 5. Similar mutational spectra are observed across all densely colonized patients. Mutational direction (ancestral to derived nucleotide) is based on the respective outgroup assigned to that patient (see Methods). Notably, Patient 26 does not show a mutational spectrum that deviates significantly from that of other patients.

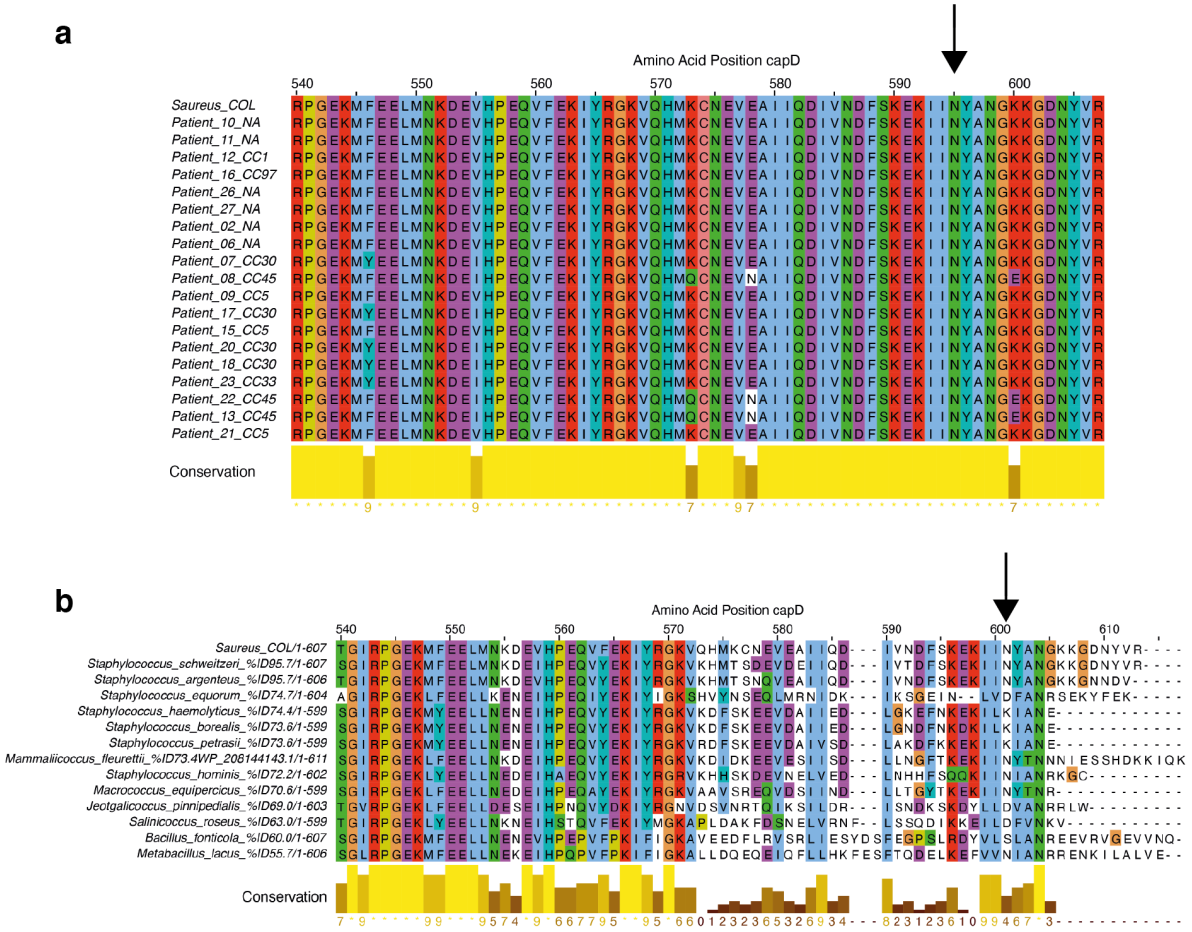

Extended Data Figure 6. Multiple sequence alignment of the terminal *capD* amino acid sequence demonstrates conservation of amino acid position 595 (arrow) within *S. aureus* but not between species. a. Multiple sequence alignment of the 607 amino acid long *capD* sequence within *Staphylococcus aureus* including the COL type strain and all *capD* sequences annotated by prokka [69] within the patient-specific pan-genome assemblies. Assigned clonal complex shown in row label (if none 'NA'). **b.** Multiple sequence alignment of *capD* across different species identified using BLAST [80]. Percent sequence identity (%ID) and aligned amino acid position is shown in each row label. Amino-acid position 595 (mutated in Pt. 09 N>S) indicated by an arrow. The multiple sequence alignments have been generated using Muscle [82] and jalview [83].

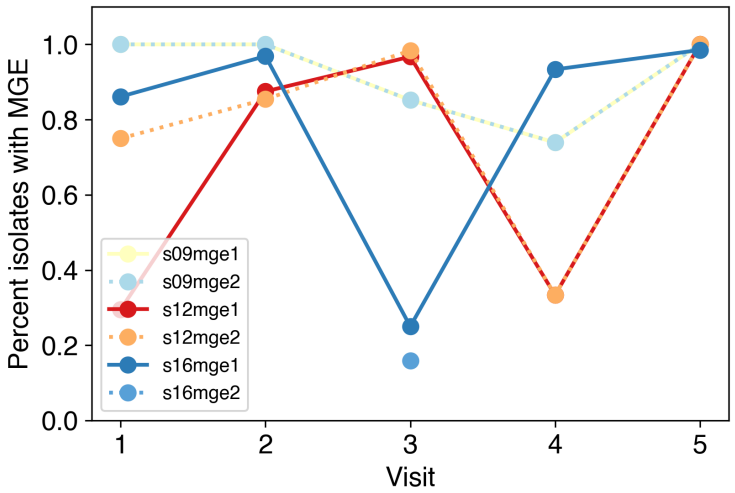

Extended Data Figure 7. Frequency of identified mobile genetic element (MGE) among isolates per visit. Isolates were considered to harbor the MGE if the mean depth across the MGE was at least half of the mean genome-wide depth. To avoid artifacts, MGEs are reported only if at least two isolates had evidence of coverage and at least two isolates had evidence of absence. All MGEs detected at the first sampling visit are present in all isolates at the last visit from the same patient. One MGE containing multiple antibiotic resistance genes in patient 16 was detected only at Visit 3. Gene annotations in each MGE are reported in **Supplementary Table 5**.

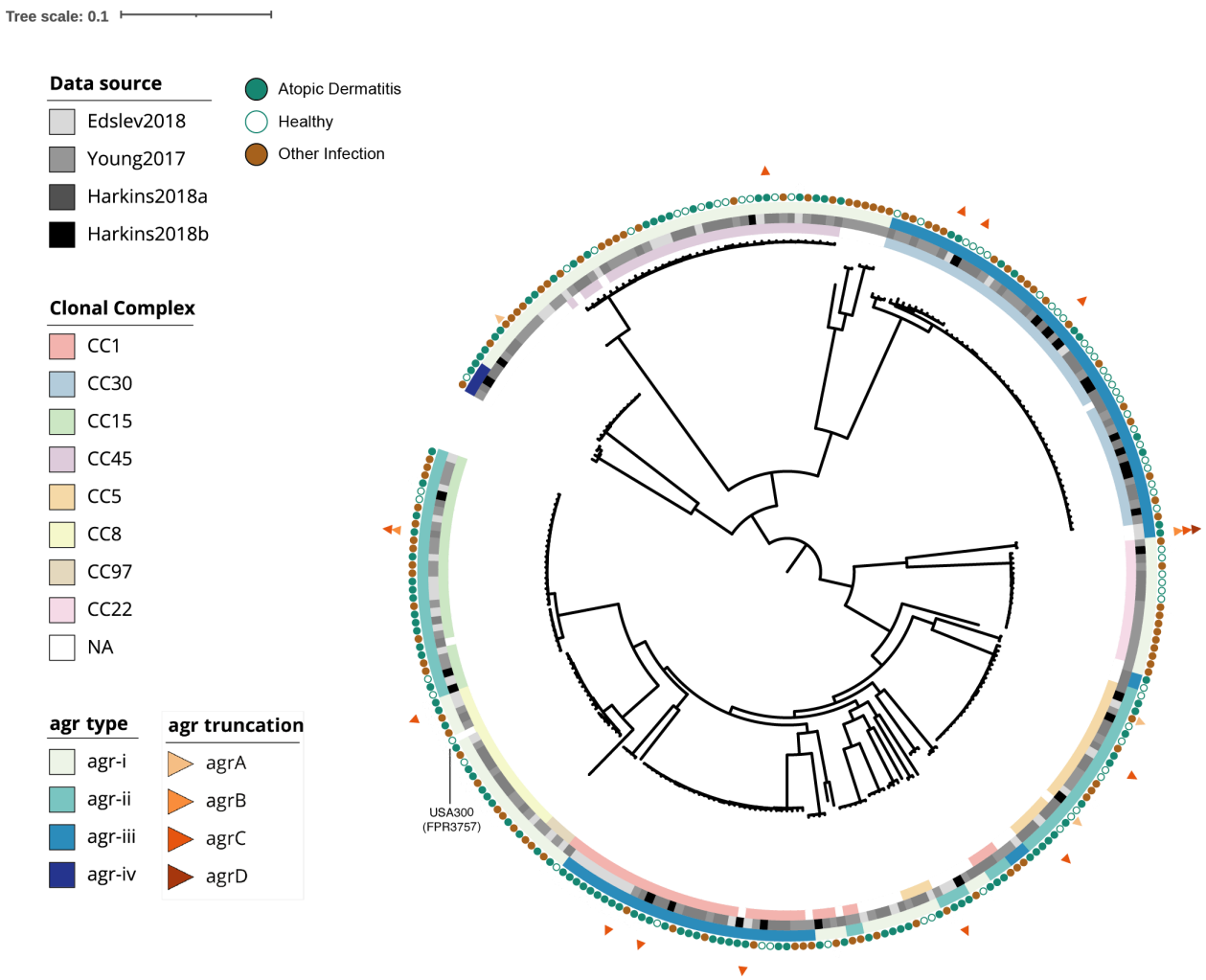

Extended Data Figure 8. Maximum-likelihood phylogeny showing relationship for all 276 *S. aureus* isolates and strain FPR3757, using a reference-based approach (similar to **Figure 3c**). Isolates are labeled with squares indicating their membership in global lineages, the study of origin, and *agr* type, with circles indicating isolation context. Triangles indicate isolates with truncated *agr A*, *B*, *C*, or/and *D*, showing 16 different independent events.

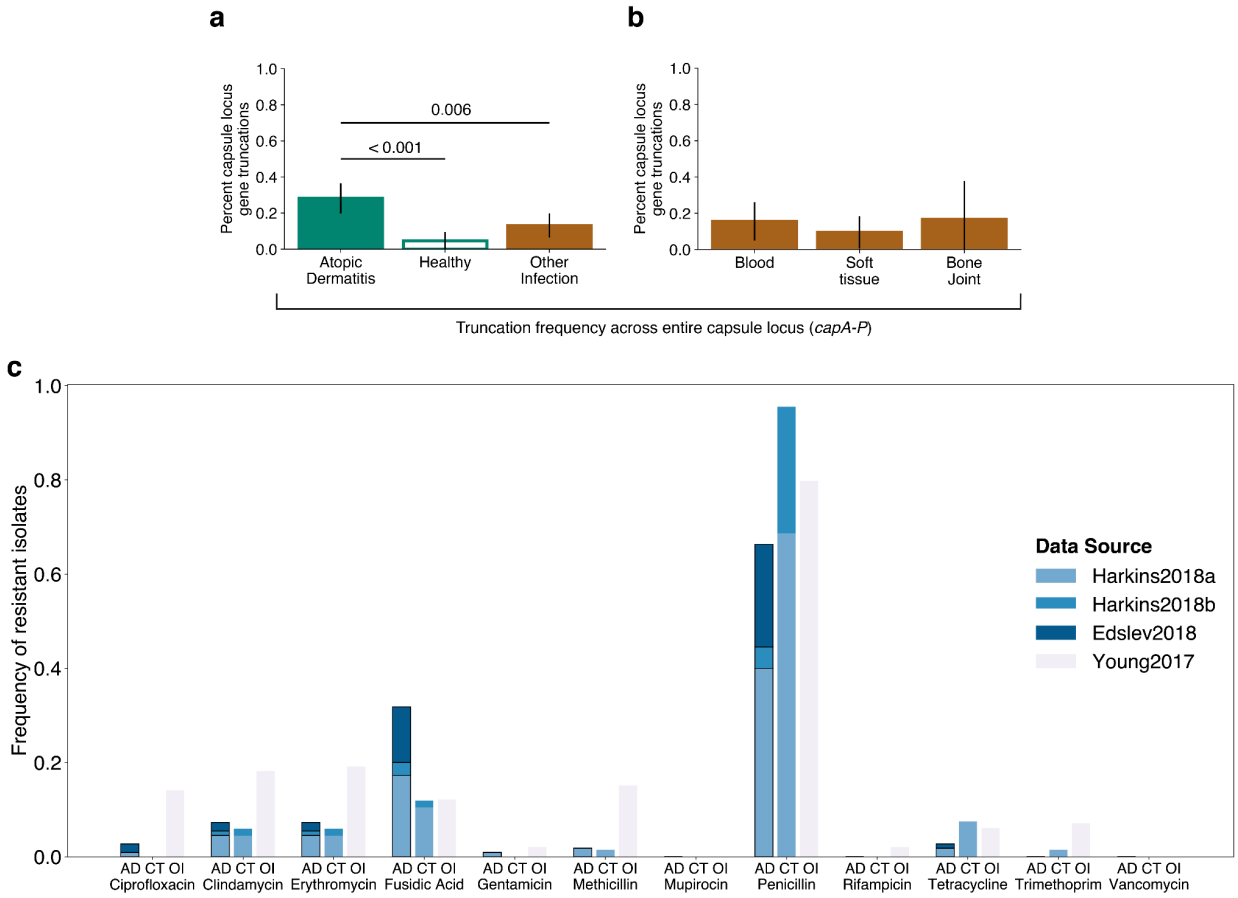

Extended Data Figure 9. Enrichment of truncations extend across the entire capsule locus in AD patients and antimicrobial resistance profile. a. Frequency of truncations in genes part of the entire capsule locus (*capA-P*) for isolates derived from individuals with atopic dermatitis, healthy, and other infections. **b.** Same as (a) but only individuals with other infections are shown and differentiated by exact type of infection. No statistical difference is observed. **c.** Frequency of antimicrobial resistance inferred in the meta-analysis of the 276 isolates from 276 individuals. Mykrobe [84] was used to predict antibiotic resistance profiles from the publicly available genomes analyzed in **Figure 3**. The percent of isolates predicted to be resistant to the displayed antibiotics are shown for isolates derived from individuals with atopic dermatitis (AD), healthy (CT), and other infections (OI).

Extended Data Figure 10. Antimicrobial sensitivity predictions for all isolates of all patients. Mykrobe [84] was used to predict antibiotic resistance profiles from all 1,587 isolates analyzed here. For each patient and visit, the percent of isolates from the major on-person lineage (black) and minor on-person lineage (gray) is shown. The percent of isolates predicted to be antibiotic resistant is shown in blue; location along the x-axis is arranged such that any vertical line within a patient reflects the same lineage isolate (i.e. resistance profiles of co-colonizing major and minor lineage can be compared). Administration of antibiotics is indicated on top of plot (see also **Supplementary Table 1**).

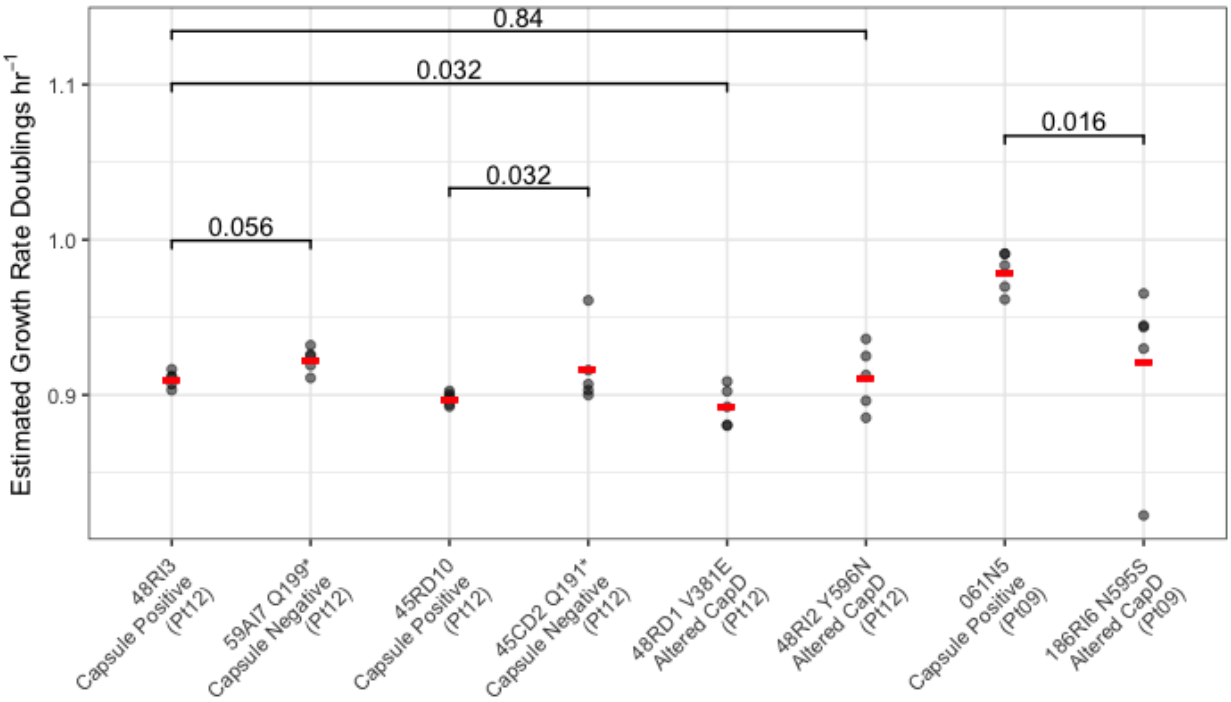

Extended Data Figure 11. Growth advantage of acapsular versus capsular isolates. Growth rates in TSB of isolates carrying *de novo* mutations in the *capD* gene as well as closely related phylogenetically basal strains (Methods), showing a growth advantage for the acapsular isolates. P-values of Wilcoxon rank sum tests shown. Strain 59-AI7 shows a 1.4% increase in growth rate over 48-RI3, and strain 45-CD2 a 2% growth rate increase over 45-RD10. Each capsule mutant was compared to the most closely related isolate in our collection, as indicated by the lines and p-values at top. Some pairs had 1-2 additional mutations outside the capsule locus, see **Supplementary Table 6.** Red lines indicate means.

a

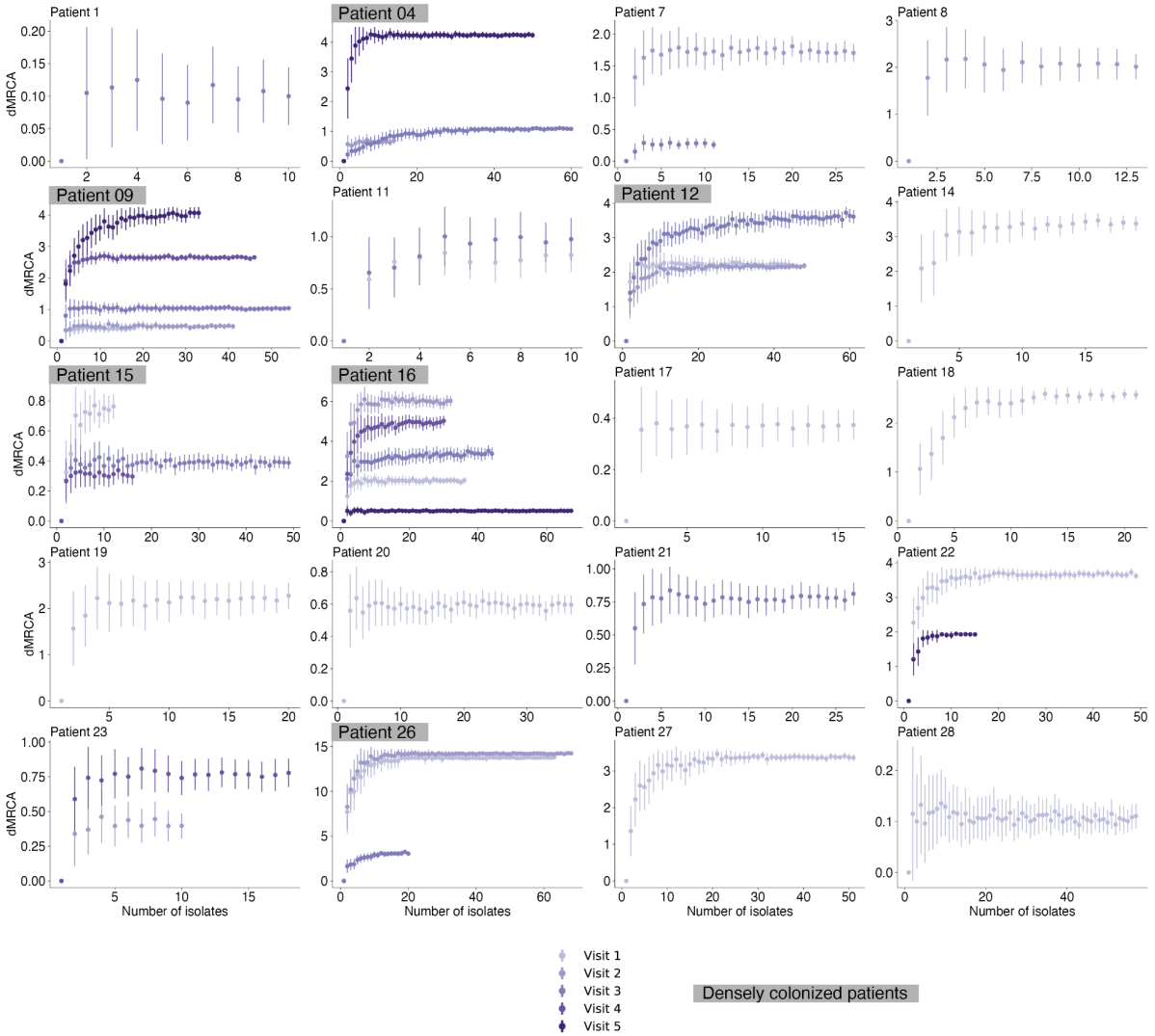
Patient 1
Patient 04
Patient 7
Patient 8
Patient 09
Patient 11
Patient 12
Patient 14
Patient 15
Patient 16
Patient 17
Patient 18
Patient 19
Patient 20
Patient 21
Patient 22
Patient 23
Patient 26
Patient 27
Patient 28
dMRCA
Number of isolates
Visit 1
Visit 2
Visit 3
Visit 4
Visit 5
Densely colonized patients

b

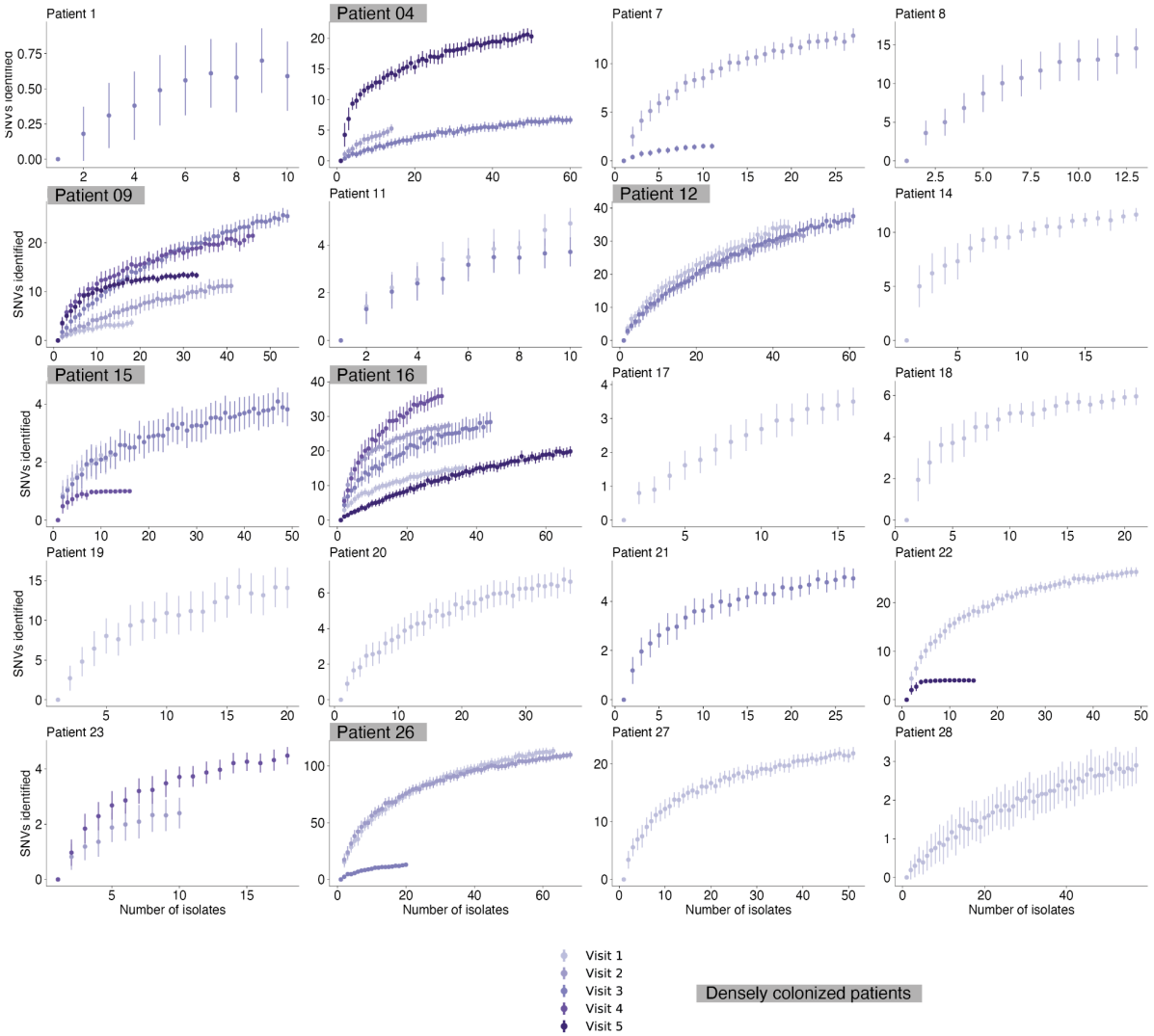

Extended Data Figure 12. Collector curves demonstrate sufficient sampling of patients intra-lineage diversity but not rare newly emerged SNVs. For each sampling point (visit) with at least 10 isolates a collector curve for (**a**) dMRCA or (**b**) identified SNVs was created, combined on a single plot per patient. For each patient-visit dataset we re-sampled with replacement 0 < x < n isolates each x sampled 100 times, calculated the within-sample diversity, and plotted the mean and standard deviation. The dMRCA results suggest sufficient sampling for most patients, whereas the SNV results suggest that rare variation remains, likely reflecting newly emerged SNVs.

Supplementary Note

Previous *in vivo* experiments with laboratory strains

In a previous version of this manuscript available on bioRxiv [85], we reported a difference between Newman WT and a Newman Cap5D deletion mutant in an epicutaneous infection model in mice. However, the two strains were found to have additional point mutations between them, including a nonsynonymous mutation in the sensor kinase *saeS* that confounded the reported impact of cap5D deletion on disease severity in this model. Here, we report only on experiments performed on strains isolated from patients, which do not demonstrate strong effect of capsule loss in mouse and tissue culture models (**Supplementary Figure 1** and **2**). Future studies are needed to show if the advantage of the acapsular phenotype *in vivo* is potentially triggered by the adaptive immune system or something on skin from people with atopic dermatitis not captured in our models.

Methods for Mouse Experiments

Bacterial Strains and Cultures for *in vivo* experiments

All experiments were performed with representative bacterial isolates carrying *de novo* mutations in the *capD* gene from patients enrolled in this study. For each test isolate, a phylogenetically closely related and basal control isolate was chosen. Sometimes the test isolate contains additional mutations compared to the most closely related basal isolate observed.

Patient 12:

Control: 048-RI3

Test: 059-AI7 (Q199* in *capD*; synonymous mutation in a hypothetical protein)

Patient 9:

Control: 061-N5

Test: 186-RI6 (N595S in *capD*; G278D ComE operon protein 3 *comEC*; intergenic mutation between two hypothetical proteins)

Bacteria were grown to stationary phase overnight at 37°C in Tryptic Soy Broth (TSB) at 250 r.p.m. Stationary phase cultures were diluted 1:100 in fresh TSB and grown for 3.5 hours to approximate mid-log phase. Cultures were then centrifuged at 800xg for 15 minutes, and the resulting pellet washed twice in phosphate buffered saline (PBS). Cells were resuspended to a concentration of ~10^{10} CFU/mL. Serial dilutions were plated on Tryptic Soy Agar (TSA) plates to confirm inoculum cell densities.

Animals

Eight-week old C57BL/6 female mice from Jackson Laboratories (Bar Harbor, ME, USA) were housed in specific pathogen free animal barrier facilities at MIT in individually ventilated isolator cages under a 12 h light/dark cycle with ad libitum food and water access. Euthanasia was performed by CO_2 inhalation.

All animal experiments were approved by the Institutional Animal Care and Use Committee (IACUC) at MIT.

Epicutaneous Skin Infection and Bacterial Load Measurements

Two days prior to epicutaneous infection, mice were shaved and the remaining hair removed using depilatory cream (Nair) along the length of their back/flank. A sterile 1 cm^2 square of gauze was soaked in 100 uL of prepared *S. aureus* inoculum (~10^9 CFU/mL for each strain, see crosshatches in figures) and applied to the flank skin. The gauze was secured using bio-occlusive film (Tegaderm, 3M) and the tape checked and repaired daily to maintain its integrity. Gauze soaked in sterile PBS was used as a control. Seven days post-inoculation, mice were euthanized by CO_2 and the dressing removed. Skin under the gauze was immediately scored for disease severity according to the following criteria: oedema (0-3), erythema (0-3), skin scale (0-3), and skin thickness (0-3) and totaled for a max skin score of "12.". A higher score indicated more severe disease/inflammation. For bacterial load, the flank skin immediately under the gauze (~1 cm^2) was excised and resuspended in 1 mL cold PBS contained in a 2 mL microcentrifuge tube. The tissue was cut into smaller pieces using sterilized scissors, two metal ball bearings (4.5 mm) were added to each tube, and the tissue was homogenized using a TissueLyser II (Qiagen, Germany) at 25 s^{-1} for 5 min. Homogenates were briefly spun down, serially diluted in PBS, and then plated for CFU counts. Bacterial identity was confirmed by plating on ChromAgar Colorex *S. aureus* (ChromAgar, France) plates to differentiate any native microbiota that may have been present. A total of two replicates were performed. The analysis of all animal experiments was blinded.

For colonization experiments, bacteria were prepared as above and ~10^7 CFU were applied to each ear in a 50 uL volume. Mice were euthanized 24 h later and tissue was harvested, homogenized, and serially diluted in PBS. Bacterial identity was confirmed by plating on ChromAgar Colorex *S. aureus* plates.

Tissue culture and intra-epithelial invasion assay

The CCD 1106 KERTr cell line (ATCC CRL-2309), comprising human epithelial keratinocytes, was seeded into flat-bottom 24-well plates in Keratinocyte Serum Free Media (Gibco) with added Keratinocytes Supplements including bovine pituitary extract and human recombinant epidermal growth factor (Gibco) and further supplemented with additional 35 ng/mL human recombinant epidermal growth factor (BD). Cells were grown at 37 C in 5% C02 until confluent. Confluent cells were washed and infected with *S. aureus* isolate strains 48-RI3, 59-AI7, 61-N5, 186-RI6. After two hours of incubation, cells were washed and cell media containing 40 ug/mL Lysostaphin (Fisher Scientific) was added and the mixture incubated for an additional hour. All strains tested were equally susceptible to killing by lysostaphin. The epithelial cells were then washed with PBS and detached by incubation with 100 uL of 0.25% Trypsin (Sigma) for 5 minutes at 37 C with 5% C02 and lysed with 400 uL of 0.1% Triton-X. Cell lysates were diluted and plated on TSA to enumerate the number of intracellular *Staphylococci*.

Supplementary Figures

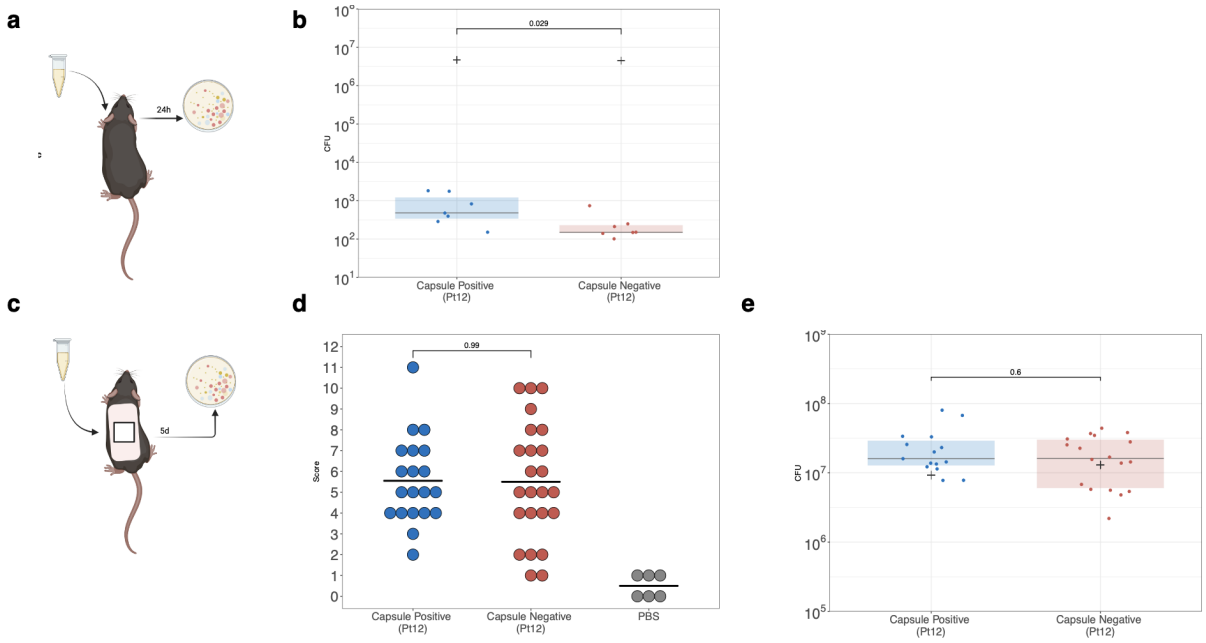

Supplementary Figure 1. Capsule absence in clinical *S. aureus* strains does not enhance virulence or colonization in *in vivo* mouse models. **a.** Colonization / adherence was assessed using a simplified version of a previously published model [1]. Bacterial strains were grown overnight, subcultured to log phase growth and washed to achieve normalized OD and applied to the ears. Bacterial load was quantified by CFU counting on ChromAgar after harvesting, homogenizing, and culturing tissue 24 h after colonization. **b.** The average recovered CFU from both ears is significantly lower (p=0.029, Wilcoxon Rank Sum) in mice treated with the capsule negative strain 059-AI7. **c.** Differences in virulence among capsular and acapsular strains was assessed using a previously published model of epicutaneous infection [86]. **d.** The composite score represents the sum of individual assessments of erythema (0-3), oedema (0-3), thickness (0-3) and scale (0-3), which demonstrates no difference between capsule and acapsular strains. **e.** Bacterial load recovered from infected skin is equivalent among clinical isolate strains. Cross represents average inoculum across three replicates, n = 5-8 mice per group per replicate. All experiments are performed using capsular (048-RI3) and acapsular (059-AI7) isolates from patient 12 and compared using a Wilcoxon rank test.

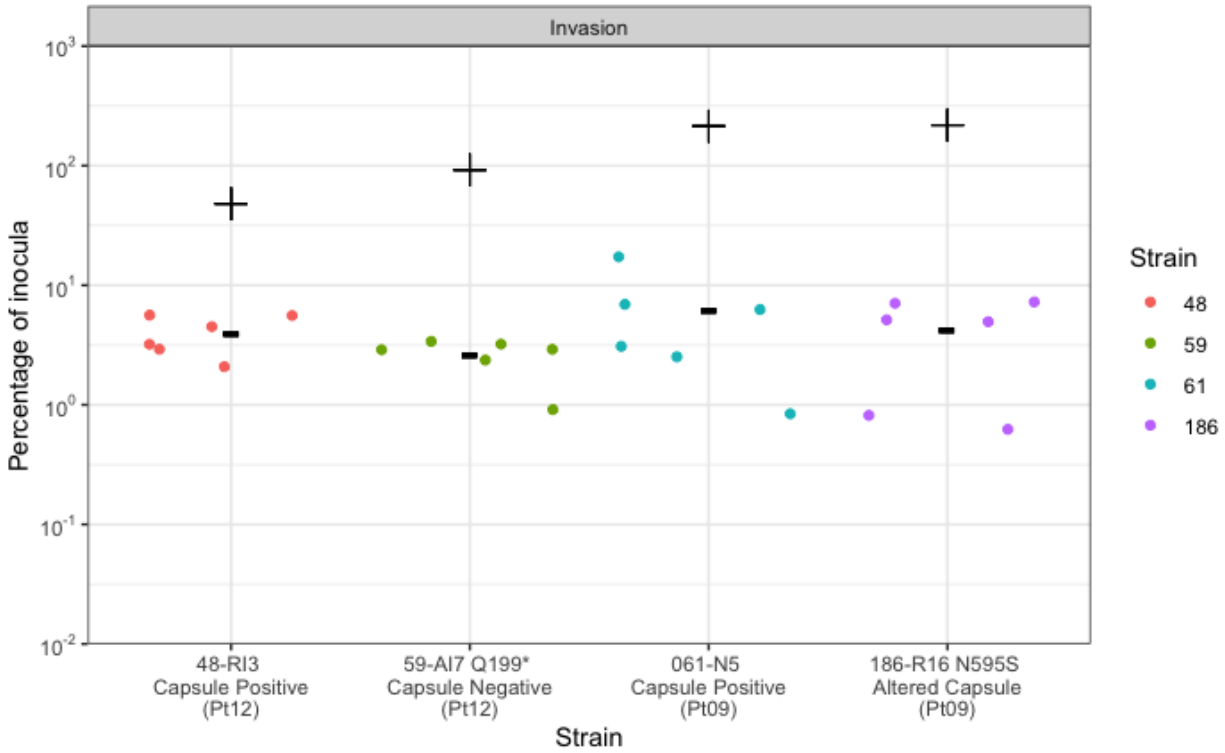

Supplementary Figure 2. Capsule positive and negative strains invade human epithelial cells at comparable rates. The percentages of log phase and overnight inocula recovered from capsule positive and negative isolates from patient 12 and patient 09 were comparable between patient strains. Crosses represent MOI.

References

1 Byrd, A. L. *et al.* Staphylococcus aureus and Staphylococcus epidermidis strain diversity underlying pediatric atopic dermatitis. *Science translational medicine* **9** (2017).

2 Palmela, C. *et al.* Adherent-invasive Escherichia coli in inflammatory bowel disease. *Gut* **67**, 574, doi:10.1136/gutjnl-2017-314903 (2018).

3 Tong, S. Y. C., Davis, J. S., Eichenberger, E., Holland, T. L. & Fowler, V. G. Staphylococcus aureus Infections: Epidemiology, Pathophysiology, Clinical Manifestations, and Management. *Clinical Microbiology Reviews* **28**, 603, doi:10.1128/CMR.00134-14 (2015).

4 Leyden, J. J., Marples, R. R. & Kligman, A. M. Staphylococcus aureus in the lesions of atopic dermatitis. *British Journal of Dermatology* **90**, 525-525, doi:https://doi.org/10.1111/j.1365-2133.1974.tb06447.x (1974).

5 Paller, A. S. *et al.* The microbiome in patients with atopic dermatitis. *Journal of Allergy and Clinical Immunology* **143**, 26-35, doi:https://doi.org/10.1016/j.jaci.2018.11.015 (2019).

6 Kong, H. H. *et al.* Temporal shifts in the skin microbiome associated with disease flares and treatment in children with atopic dermatitis. *Genome Research* **22**, 850-859 (2012).

7 Schultz Larsen, F., Holm, N. V. & Henningsen, K. Atopic dermatitis: A genetic-epidemiologic study in a population-based twin sample. *Journal of the American Academy of Dermatology* **15**, 487-494, doi:https://doi.org/10.1016/S0190-9622(86)70198-9 (1986).

8 Paternoster, L. *et al.* Multi-ancestry genome-wide association study of 21,000 cases and 95,000 controls identifies new risk loci for atopic dermatitis. *Nature genetics* **47**, 1449 (2015).

9 Huang, J. T., Abrams, M., Tlougan, B., Rademaker, A. & Paller, A. S. Treatment of Staphylococcus aureus colonization in atopic dermatitis decreases disease severity. *Pediatrics* **123**, e808-e814 (2009).

10 Lieberman, T. D. *et al.* Parallel bacterial evolution within multiple patients identifies candidate pathogenicity genes. *Nat Genet* **43**, 1275-1280, doi:10.1038/ng.997 (2011).

11 Snitkin, E. S. *et al.* Genomic insights into the fate of colistin resistance and Acinetobacter baumannii during patient treatment. *Genome research* **23**, 1155-1162, doi:10.1101/gr.154328.112 (2013).

12 Ernst, C. M. *et al.* Adaptive evolution of virulence and persistence in carbapenem-resistant Klebsiella pneumoniae. *Nature medicine* **26**, 705-711 (2020).

13 Zhao, S. *et al.* Adaptive evolution within gut microbiomes of healthy people. *Cell host & microbe* **25**, 656-667 (2019).

14 Williams, M. R. & Gallo, R. L. The Role of the Skin Microbiome in Atopic Dermatitis. *Current Allergy and Asthma Reports* **15**, 65, doi:10.1007/s11882-015-0567-4 (2015).

15 Ni, J., Wu, G. D., Albenberg, L. & Tomov, V. T. Gut microbiota and IBD: causation or correlation? *Nature reviews Gastroenterology & hepatology* **14**, 573 (2017).

16 Nakatsuji, T. *et al.* Antimicrobials from human skin commensal bacteria protect against Staphylococcus aureus and are deficient in atopic dermatitis. *Science translational medicine* **9** (2017).

17 Hall, A. B. *et al.* A novel Ruminococcus gnavus clade enriched in inflammatory bowel disease patients. *Genome Medicine* **9**, 103, doi:10.1186/s13073-017-0490-5 (2017).

18 Asher, M. I. *et al.* Worldwide time trends in the prevalence of symptoms of asthma, allergic rhinoconjunctivitis, and eczema in childhood: ISAAC Phases One and Three repeat multicountry cross-sectional surveys. *The Lancet* **368**, 733-743, doi:https://doi.org/10.1016/S0140-6736(06)69283-0 (2006).

19 Hay, R. J. *et al.* The Global Burden of Skin Disease in 2010: An Analysis of the Prevalence and Impact of Skin Conditions. *Journal of Investigative Dermatology* **134**, 1527-1534, doi:https://doi.org/10.1038/jid.2013.446 (2014).

20 Baurecht, H. *et al.* Epidermal lipid composition, barrier integrity, and eczematous inflammation are associated with skin microbiome configuration. *Journal of Allergy and Clinical Immunology* **141**, 1668-1676.e1616, doi:https://doi.org/10.1016/j.jaci.2018.01.019 (2018).

21 Tauber, M. *et al.* Staphylococcus aureus density on lesional and nonlesional skin is strongly associated with disease severity in atopic dermatitis. *Journal of Allergy and Clinical Immunology* **137**, 1272-1274 (2016).
22 Khadka, V. D. *et al.* The Skin Microbiome of Patients With Atopic Dermatitis Normalizes Gradually During Treatment. *Frontiers in Cellular and Infection Microbiology* **11**, doi:10.3389/fcimb.2021.720674 (2021).
23 Gorwitz, R. J. *et al.* Changes in the Prevalence of Nasal Colonization with Staphylococcus aureus in the United States, 2001–2004. *The Journal of Infectious Diseases* **197**, 1226-1234, doi:10.1086/533494 (2008).
24 Oh, J. *et al.* Biogeography and individuality shape function in the human skin metagenome. *Nature* **514**, 59-64, doi:10.1038/nature13786 (2014).
25 Enright, M. C. *et al.* The evolutionary history of methicillin-resistant Staphylococcus aureus (MRSA). *Proceedings of the National Academy of Sciences* **99**, 7687-7692 (2002).
26 Nakamura, Y. *et al.* Staphylococcus Agr virulence is critical for epidermal colonization and associates with atopic dermatitis development. *Science Translational Medicine* **12**, eaay4068, doi:10.1126/scitranslmed.aay4068 (2020).
27 Harkins, C. P. *et al.* The Microevolution and Epidemiology of Staphylococcus aureus Colonization during Atopic Eczema Disease Flare. *Journal of Investigative Dermatology* **138**, 336-343, doi:https://doi.org/10.1016/j.jid.2017.09.023 (2018).
28 Chopra, R. *et al.* Severity strata for Eczema Area and Severity Index (EASI), modified EASI, Scoring Atopic Dermatitis (SCORAD), objective SCORAD, Atopic Dermatitis Severity Index and body surface area in adolescents and adults with atopic dermatitis. *British Journal of Dermatology* **177**, 1316-1321 (2017).
29 Holden, M. T. *et al.* A genomic portrait of the emergence, evolution, and global spread of a methicillin-resistant Staphylococcus aureus pandemic. *Genome Res* **23**, 653-664, doi:10.1101/gr.147710.112 (2013).
30 McAdam, P. R. *et al.* Molecular tracing of the emergence, adaptation, and transmission of hospital-associated methicillin-resistant Staphylococcus aureus. *Proceedings of the National Academy of Sciences of the United States of America* **109**, 9107-9112, doi:10.1073/pnas.1202869109 (2012).
31 Nübel, U. *et al.* MRSA Transmission on a Neonatal Intensive Care Unit: Epidemiological and Genome-Based Phylogenetic Analyses. *PloS one* **8**, e54898, doi:10.1371/journal.pone.0054898 (2013).
32 Uhlemann, A. C. *et al.* Molecular tracing of the emergence, diversification, and transmission of S. aureus sequence type 8 in a New York community. *Proc Natl Acad Sci U S A* **111**, 6738-6743, doi:10.1073/pnas.1401006111 (2014).
33 Young, B. C. *et al.* Evolutionary dynamics of Staphylococcus aureus during progression from carriage to disease. *Proc Natl Acad Sci U S A* **109**, 4550-4555, doi:10.1073/pnas.1113219109 (2012).
34 Golubchik, T. *et al.* Within-Host Evolution of Staphylococcus aureus during Asymptomatic Carriage. *PloS one* **8**, e61319, doi:10.1371/journal.pone.0061319 (2013).
35 Turner, N. A. *et al.* Methicillin-resistant Staphylococcus aureus: an overview of basic and clinical research. *Nature Reviews Microbiology* **17**, 203-218 (2019).
36 Lieberman, T. D. *et al.* Genetic variation of a bacterial pathogen within individuals with cystic fibrosis provides a record of selective pressures. *Nat Genet* **46**, 82-87, doi:10.1038/ng.2848 (2014).
37 O'Riordan, K. & Lee, J. C. Staphylococcus aureus capsular polysaccharides. *Clinical microbiology reviews* **17**, 218-234 (2004).
38 Kuipers, A. *et al.* The Staphylococcus aureus polysaccharide capsule and Efb-dependent fibrinogen shield act in concert to protect against phagocytosis. *Microbiology* **162**, 1185 (2016).

39 Verbrugh, H. A., Peterson, P. K., Nguyen, B. Y., Sisson, S. P. & Kim, Y. Opsonization of encapsulated Staphylococcus aureus: the role of specific antibody and complement. *The Journal of Immunology* **129**, 1681-1687 (1982).
40 Boyle-Vavra, S. *et al.* USA300 and USA500 clonal lineages of Staphylococcus aureus do not produce a capsular polysaccharide due to conserved mutations in the cap5 locus. *mBio* **6** (2015).
41 Mohamed, N. *et al.* Molecular epidemiology and expression of capsular polysaccharides in Staphylococcus aureus clinical isolates in the United States. *PloS one* **14**, e0208356, doi:10.1371/journal.pone.0208356 (2019).
42 Pöhlmann-Dietze, P. *et al.* Adherence of Staphylococcus aureus to endothelial cells: influence of capsular polysaccharide, global regulator agr, and bacterial growth phase. *Infection and immunity* **68**, 4865-4871, doi:10.1128/iai.68.9.4865-4871.2000 (2000).
43 Risley, A. L., Loughman, A., Cywes-Bentley, C., Foster, T. J. & Lee, J. C. Capsular Polysaccharide Masks Clumping Factor A-Mediated Adherence of Staphylococcus aureus to Fibrinogen and Platelets. *The Journal of Infectious Diseases* **196**, 919-927, doi:10.1086/520932 (2007).
44 Tuchscherr, L. P. *et al.* Capsule-negative Staphylococcus aureus induces chronic experimental mastitis in mice. *Infect Immun* **73**, 7932-7937, doi:10.1128/iai.73.12.7932-7937.2005 (2005).
45 Young, B. C. *et al.* Severe infections emerge from commensal bacteria by adaptive evolution. *elife* **6**, e30637 (2017).
46 Edslev, S. M., Clausen, M.-L., Agner, T., Stegger, M. & Andersen, P. S. Genomic analysis reveals different mechanisms of fusidic acid resistance in Staphylococcus aureus from Danish atopic dermatitis patients. *Journal of Antimicrobial Chemotherapy* **73**, 856-861 (2018).
47 Harkins, C. P. *et al.* The widespread use of topical antimicrobials enriches for resistance in Staphylococcus aureus isolated from patients with atopic dermatitis. *British Journal of Dermatology* **179**, 951-958, doi:https://doi.org/10.1111/bjd.16722 (2018).
48 Lei, M. G. & Lee, C. Y. MgrA Activates Staphylococcal Capsule via SigA-Dependent Promoter. *Journal of Bacteriology* **203**, e00495-00420, doi:10.1128/JB.00495-20 (2020).
49 Keinhörster, D., George, S. E., Weidenmaier, C. & Wolz, C. Function and regulation of Staphylococcus aureus wall teichoic acids and capsular polysaccharides. *International Journal of Medical Microbiology* **309**, 151333, doi:https://doi.org/10.1016/j.ijmm.2019.151333 (2019).
50 Luong, T., Sau, S., Gomez, M., Lee, J. C. & Lee, C. Y. Regulation of Staphylococcus aureus capsular polysaccharide expression by agr and sarA. *Infection and immunity* **70**, 444-450 (2002).
51 Shinefield, H. *et al.* Use of a Staphylococcus aureus Conjugate Vaccine in Patients Receiving Hemodialysis. *New England Journal of Medicine* **346**, 491-496, doi:10.1056/NEJMoa011297 (2002).
52 Tuchscherr, L. P. N., Buzzola, F. R., Alvarez, L. P., Lee, J. C. & Sordelli, D. O. Antibodies to Capsular Polysaccharide and Clumping Factor A Prevent Mastitis and the Emergence of Unencapsulated and Small-Colony Variants of Staphylococcus aureus in Mice. *Infection and Immunity* **76**, 5738-5744, doi:doi:10.1128/IAI.00874-08 (2008).
53 Debray, R. *et al.* Priority effects in microbiome assembly. *Nature Reviews Microbiology* **20**, 109-121, doi:10.1038/s41579-021-00604-w (2022).
54 Suligoy, C. M. *et al.* Acapsular Staphylococcus aureus with a non-functional agr regains capsule expression after passage through the bloodstream in a bacteremia mouse model. *Scientific Reports* **10**, 14108, doi:10.1038/s41598-020-70671-1 (2020).
55 Lou, Y. C. *et al.* Using strain-resolved analysis to identify contamination in metagenomics data. *bioRxiv*, 2022.2001.2016.476537, doi:10.1101/2022.01.16.476537 (2022).
56 Hanifin, J. M. Diagnostic features of atopic dermatitis. *Acta Derm. Venereol.* **92**, 44-47 (1980).
57 Baym, M. *et al.* Inexpensive multiplexed library preparation for megabase-sized genomes. *PloS one* **10**, e0128036, doi:10.1371/journal.pone.0128036 (2015).
58 Martin, M. Cutadapt removes adapter sequences from high-throughput sequencing reads. *EMBnet. journal* **17**, 10-12 (2011).

59 Joshi, N. A. & Fass, J. N. Sickle: a sliding-window, adaptive, quality-based trimming tool for FastQ files. (2011).
60 Li, H. & Durbin, R. Fast and accurate short read alignment with Burrows–Wheeler transform. *Bioinformatics* **25**, 1754-1760, doi:10.1093/bioinformatics/btp324 (2009).
61 Molder, F. *et al.* Sustainable data analysis with Snakemake [version 1; peer review: 1 approved, 1 approved with reservations]. *F1000Research* **10**, doi:10.12688/f1000research.29032.1 (2021).
62 Stamatakis, A. RAxML version 8: a tool for phylogenetic analysis and post-analysis of large phylogenies. *Bioinformatics* **30**, 1312-1313, doi:10.1093/bioinformatics/btu033 (2014).
63 Letunic, I. & Bork, P. Interactive Tree Of Life (iTOL) v5: an online tool for phylogenetic tree display and annotation. *Nucleic acids research* **49**, W293-W296 (2021).
64 Inouye, M. *et al.* SRST2: Rapid genomic surveillance for public health and hospital microbiology labs. *Genome Medicine* **6**, 90, doi:10.1186/s13073-014-0090-6 (2014).
65 Jolley, K. A., Bray, J. E. & Maiden, M. C. J. Open-access bacterial population genomics: BIGSdb software, the PubMLST.org website and their applications. *Wellcome Open Res* **3**, 124, doi:10.12688/wellcomeopenres.14826.1 (2018).
66 Singh, M. *et al.* Complete genome sequence of the drug-naive classical Staphylococcus aureus strain FDA209P. *Genome Announcements* **3**, e01343-01315 (2015).
67 Wood, D. E., Lu, J. & Langmead, B. Improved metagenomic analysis with Kraken 2. *Genome biology* **20**, 1-13 (2019).
68 Bankevich, A. *et al.* SPAdes: a new genome assembly algorithm and its applications to single-cell sequencing. *Journal of computational biology : a journal of computational molecular cell biology* **19**, 455-477, doi:10.1089/cmb.2012.0021 (2012).
69 Seemann, T. Prokka: rapid prokaryotic genome annotation. *Bioinformatics* **30**, 2068-2069, doi:10.1093/bioinformatics/btu153 (2014).
70 Langmead, B. & Salzberg, S. L. Fast gapped-read alignment with Bowtie 2. *Nature methods* **9**, 357 (2012).
71 Felsenstein, J. *PHYLIP (phylogeny inference package), version 3.5 c*. (Joseph Felsenstein., 1993).
72 Pritchard, J. K., Pickrell, J. K. & Coop, G. The Genetics of Human Adaptation: Hard Sweeps, Soft Sweeps, and Polygenic Adaptation. *Current Biology* **20**, R208-R215, doi:10.1016/j.cub.2009.11.055 (2010).
73 Garud, N. R., Good, B. H., Hallatschek, O. & Pollard, K. S. Evolutionary dynamics of bacteria in the gut microbiome within and across hosts. *PLoS biology* **17**, e3000102 (2019).
74 Lang, G. I., Botstein, D. & Desai, M. M. Genetic variation and the fate of beneficial mutations in asexual populations. *Genetics* **188**, 647-661 (2011).
75 Fu, L., Niu, B., Zhu, Z., Wu, S. & Li, W. CD-HIT: accelerated for clustering the next-generation sequencing data. *Bioinformatics* **28**, 3150-3152 (2012).
76 Noble, R. (2019).
77 Sagulenko, P., Puller, V. & Neher, R. A. TreeTime: Maximum-likelihood phylodynamic analysis. *Virus Evolution* **4**, vex042, doi:10.1093/ve/vex042 (2018).
78 Virtanen, P. *et al.* SciPy 1.0: fundamental algorithms for scientific computing in Python. *Nature Methods* **17**, 261-272, doi:10.1038/s41592-019-0686-2 (2020).
79 Lee, J. C., Liu, M. J., Parsonnet, J. & Arbeit, R. D. Expression of type 8 capsular polysaccharide and production of toxic shock syndrome toxin 1 are associated among vaginal isolates of Staphylococcus aureus. *Journal of Clinical Microbiology* **28**, 2612-2615, doi:10.1128/jcm.28.12.2612-2615.1990 (1990).
80 Madden, T. in *The NCBI Handbook [Internet]. 2nd edition* (National Center for Biotechnology Information (US), 2013).
81 Jarraud, S. *et al.* Exfoliatin-producing strains define a fourth agr specificity group in Staphylococcus aureus. *J Bacteriol* **182**, 6517-6522, doi:10.1128/jb.182.22.6517-6522.2000 (2000).

82 Edgar, R. C. MUSCLE: multiple sequence alignment with high accuracy and high throughput. *Nucleic acids research* **32**, 1792-1797 (2004).
83 Waterhouse, A. M., Procter, J. B., Martin, D. M. A., Clamp, M. & Barton, G. J. Jalview Version 2—a multiple sequence alignment editor and analysis workbench. *Bioinformatics* **25**, 1189-1191, doi:10.1093/bioinformatics/btp033 (2009).
84 Hunt, M. *et al.* Antibiotic resistance prediction for Mycobacterium tuberculosis from genome sequence data with Mykrobe. *Wellcome open research* **4**, 191-191, doi:10.12688/wellcomeopenres.15603.1 (2019).
85 Key, F. M. *et al.* On-person adaptive evolution of Staphylococcus aureus during atopic dermatitis increases disease severity. *bioRxiv*, 2021.2003.2024.436824, doi:10.1101/2021.03.24.436824 (2021).
86 Nakamura, Y. *et al.* Staphylococcus δ-toxin induces allergic skin disease by activating mast cells. *Nature* **503**, 397-401, doi:10.1038/nature12655 (2013).